Production of $CoFe_2O_4$/Natural Organic Matter (NOM) Nanocomposite from Iron Mining Wastes to Remove Some Variety of Polymer Types, Including Polyethylene, Polypropylene, Polystyrene and Polyvinyl Chloride

RUKİYE ÖZTEKİN [a], DELİA TERESA SPONZA [a,*]
[a] Department of Environmental Engineering
Dokuz Eylül University
Tınaztepe Campus, 35160 Buca/Izmir,
TURKEY
*Corresponding Author

Abstract: - In this study, a hybrid cobalt ferrite doped natural organic matter ($CoFe_2O_4$/NOM) nanocomposite (NC) was generated from iron ions recovered from iron ore mining tailings using as precursors. The products were evaluated in terms of their potential for the catalytic reduction of Polyethylene (PE), Polypropylene (PP), Polystyrene (PS) and Polyvinyl chloride (PVC) nanoplastics. The characteristics of the synthesized $CoFe_2O_4$/NOM NCs were assessed using XRD, FTIR, FESEM, HRTEM, and VSM analyses, respectively. PE is a member of the important family of polyolefin resins. PP is slightly harder and more heat-resistant compared to PE. PS is a synthetic polymer made from monomers of the aromatic hydrocarbon styrene. PVC is the world's third-most widely produced synthetic polymer of plastic after PE and PP polymers. For maximum PE, PP, PS and PVC polymers yields (99.20 and 99.90%) the optimized conditions were as follows: a $CoFe_2O_4$/NOM NC concentration of 10 mg/l, a $CoFe_2O_4$ to NOM ratio of 4.2%, a contact time of 30 min, a pH of 7.0, a sunlight power of 30 W/m^2 and a temperature of 30°C. Increasing the contact time from 5 to 30 min led to an increase in photooxidation efficiencies of PE, PP, PS and PVC polymers from around 80-90% to 99.90% and 99.20%, respectively. Reusability studies for $CoFe_2O_4$/NOM exhibited high yields during ten cycles with the same yields obtained in the first cycle (99.90% for PE; PP and PS and 99.20% for PVC).

Key-Words: - Iron mining wastes; Magnetic hybrid cobalt spinel ferrite doped natural organic matter ($CoFe_2O_4$/NOM); Nanocomposites; Nanoplastics; Polyethylene (PE); Polymer; Polypropylene (PP); Polystyrene (PS); Polyvinyl Chloride (PVC).

Received: April 19, 2025. Revised: June 26, 2025. Accepted: July 22, 2025. Published: September 1, 2025.

1 Introduction

Nanoplastics are created when everyday products such as clothes, food and beverage packaging, home furnishings, plastic bags, toys and toiletries degrade. This can be caused by environmental factors such as sunlight or wear and tear from mechanical action. Many personal care products, such as scrubs and shampoos, can also release nanoplastics.

Like larger plastic particles, nanoplastics can come from a variety of polymer types, including polyethylene (PE), polypropylene (PP), polystyrene (PS) and polyvinyl chloride (PVC). Because, plastic products are widely used, it is hard to avoid nanoplastics in our daily lives.

When plastics reach the nanoscale, they present unique questions and challenges because of their tiny size and varying surface properties and composition. Since nanoplastics are small, they can easily penetrate cells and tissues that larger particles cannot. If they accumulate within living organisms, they could potentially cause adverse biological effects. It is well known that larger plastic debris can fragment into nanoplastics, but there is much to learn about how these fragments degrade further. Researchers are working to detect and understand nanoplastics across many environments so that they can develop effective strategies to manage and mitigate these materials' effects on people and the planet.

Polyethylene (PE), light, versatile synthetic resin made from the polymerization of ethylene. PE is a member of the important family of polyolefin resins. It is the most widely used plastic in the world, being made into products ranging from clear food wrap and shopping bags to detergent bottles and automobile fuel tanks. It can also be slit or spun into synthetic fibres or modified to take on the elastic properties of a rubber. Ethylene (C_2H_4) is a gaseous hydrocarbon commonly produced by the cracking of ethane, which in turn is a major constituent of natural gas or can be distilled from petroleum. C_2H_4 molecules are essentially composed of two methylene units (CH_2) linked together by a double bond between the carbon atoms a structure represented by the formula CH_2=CH_2. Under the influence of polymerization catalysts, the double bond can be broken and the resultant extra single bond used to link to a carbon atom in another C_2H_4 molecule. This simple structure, repeated thousands of times in a single molecule, is the key to the properties of PE. The long, chainlike molecules, in which hydrogen atoms are connected to a carbon backbone, can be produced in linear or branched forms ranched versions are known as low-density polyethylene (LDPE) or linear low-density polyethylene (LLDPE); linear versions are known as high-density polyethylene (HDPE) and ultrahigh-molecular-weight polyethylene (UHMWPE). The basic PE composition can be modified by the inclusion of other elements or chemical groups, as in the case of chlorinated and chlorosulfonated PE. In addition to, C_2H_4 can be copolymerized with other monomers such as vinyl acetate or propylene to produce a number of C_2H_4 copolymers. The main commercial resins (PET-polyethylene terephthalate (PET); HDPE, PVC, LDPE, PP, and PS among others of the industrial plastics and their properties were summarized earlier, [1], [2]. The resin diversity and the integration of plastics in composite materials such as metal-plastic, glass-plastic, and fiber-plastic that are difficult to be disassemble complicate the recycling of end-of-life plastics. Therefore, given strict environmental concerns and increasing public pressure, the landfill rate of plastic waste is expected to be significantly reduced, while the incineration and recycling rates will increase over the coming decades, [3].

Polypropylene (PP), (known as polypropene), is a thermoplastic polymer used in a wide variety of applications. PP is produced via chain-growth polymerization from the monomer propylene. PP belongs to the group of polyolefins, and is partially crystalline and non-polar. PP's properties are similar to PE, but PP is slightly harder and more heat-resistant. PP is a white, mechanically rugged material and has a high chemical resistance, [4]. PP is the second-most widely produced commodity plastic after PE, [5]. Recently, PP has been received as a potential polymer matrix for magnetic and dielectric nanoparticle fillers to fabricate advanced nanocomposites for electromagnetic interference shielding applications. The nanocomposites of PP in-situ reduced graphene oxide (GO) with outstanding electromagnetic interference shielding characteristics, [6]. The lightweight PP/stainless-steel fiber composite foam is excellent for electromagnetic interference shielding, [7]. In addition, The PP/carbon fiber composite foams are outstanding for electromagnetic interference shielding applications, [8]. The carbon fibers in PP matrix composites and their electromagnetic interference shielding characteristics, [9].

Polystyrene (PS) is a synthetic polymer made from monomers of the aromatic hydrocarbon styrene, [10]. PS can be solid or foamed. Generaly, PS is clear, hard, and brittle. PS is an inexpensive resin per unit weight. PS is a poor barrier to air and water vapor and has a relatively low melting point, [11]. PS is one of the most widely used plastics, with the scale of its production being several million tonnes per year, [12]. PS is naturally transparent, but can be colored with colorants. Uses include protective packaging, for example packing peanuts and optical disc jewel cases, and also, containers, lids, bottles, trays, tumblers, disposable cutlery, etc., [11], in the making of models, and as an alternative material for phonograph records, [13]. As a thermoplastic polymer, PS is in a solid (glassy) state at 25ºC room temperature but flows if heated above about 100°C, PS's glass transition temperature. It becomes rigid again when cooled. This temperature behaviour is exploited for extrusion as in Styrofoam, and also for molding and vacuum forming, since it can be cast into molds with fine detail. The temperatures behavior can be controlled by photocrosslinking, [12]. Under ASTM standards, PS is regarded as not biodegradable. PS is accumulating as a form of litter in the outside environment, particularly along shores and waterways, especially in its foam form, and in the Pacific Ocean, [13]. Recently, polymers including polyethylene glycol (PEG), PS, polyvinyl alcohol (PVA), polyvinylpyrrolidone (PVP), polyaniline (PA) and polyvinylidene fluoride (PVDF) have been incorporated during or after the preparation of $CoFe_2O_4$ NPs to avoid the agglomeration between the magnetic nanoparticles. This process tunes the physicochemical properties of nanoparticles through controlling their size and morphology, [14], [15], [16], [17], [18], [19]. Among the many polymers used in the synthesis of $CoFe_2O_4$ NPs, PS has been extensively used due to its positive CH_2 groups, ability to control the size and shape of the nanoparticles, relatively low cost and easy synthesis process. Even though, several reports are available on the synthesis and characterization of PS and various polymers coated magnetic $CoFe_2O_4$ NPs, to the best our knowledge, no report is focused on the preparation and characterization of $CoFe_2O_4$ NPs by coprecipitation method adding various concentrations of PS. Magnetic $CoFe_2O_4$ NPs were prepared by co-precipitation method using various concentrations of PS as surfactant and the influence of various concentrations of PS on the structural, morphological, dielectric and magnetic properties of $CoFe_2O_4$ NPs is reported, [20].

Polyvinyl chloride (PVC) [poly(vinyl chloride)] is the world's third-most widely produced synthetic polymer of plastic (after PE and PP), [21]. PVC comes in rigid (RPVC) and flexible forms. RPVC is used in construction for pipes, doors and windows, making plastic bottles, packaging, and bank or membership cards. Adding plasticizers makes PVC softer and more flexible. PVC is used in plumbing, electrical cable insulation, flooring, signage, phonograph records, inflatable products, and in rubber substitutes, etc., [21]. PVC is used in the production of canvas with cotton or linen. PVC is a white, brittle solid, and soluble in ketones, chlorinated solvents, dimethylformamide (DMF), tetrahydrofuran (THF) and dimethylacetamide (DMAc or DMA), [22]. The chlorine content of PVC plastics is a drawback and such plastics cannot be directly used for Fe-oxides reduction because a part of the iron will be transformed into chlorides at a high temperature. Recent research reports suggested the de-chlorination of PVC can be performed by hydrothermal methods in an alkaline system, [23], [24], [25], as well as by the thermal route, [26], [27], [28], [29]. Their results agreed that HCl is the initial-bearing chlorine product during PVC treatment by dry methods. PVC is frequently selected for its affordability, robust mechanical characteristics, resistance to fire, and chemical resilience. PVC is commonly employed as insulation in the construction of power lines. Polymers like PVC are favored for their cost-effectiveness, ease of manufacturing, and resilience as thermoplastic materials for insulation. The pliability and advantageous chemical and dielectric characteristics of PVC render it an ideal choice as the base material in composites, [30]. As a result, $CoFe_2O_4$ NPs was carried out in order to achieve a harmonious equilibrium between dielectric and magnetic loss, with the objective of enhancing the permittivity and permeability of the composite material. Magnetic ferrites are frequently utilized for wave absorption as they offer a cost-effective, easily fabricated, and highly efficient absorption solution. In addition to, the limited electrical insulation abilities of unadulterated ferrite pose a challenge due to its narrow absorption spectrum which may not be pragmatic for real-world use. By amalgamating ferrite with suitable dielectric substances, these constraints can be effectively mitigated. The interplay of magnetic forces between neighboring $CoFe_2O_4$ NPs resulted in alterations to their magnetic properties, ultimately enhancing the electromagnetic absorption capabilities in the Bamboo-derived carbon/NiS_2/$(CoFe_2O_4)x$/PVC metacomposites, [31].

The mining and extraction of iron are vital in the global economy, since many sectors of industry are highly dependent on this raw material. According to UNICTAD (United Nations Conference on Trade and Development), iron ore is the mineral extracted from the environment in the greatest quantities, with the largest reserves found in Australia, Brazil, and China, [32].

Intensive iron mining activities produce large amounts of hazardous wastes that typically have high contents of acid-generating sulfide minerals and potentially toxic metals, [33], [34]. As a result, these mining activities can lead to high levels of environmental degradation, water and soil contamination, and biodiversity loss, [35].

The main waste produced by this activity is the sludge resulting from the stages of fragmentation and concentration of the ore, consisting of fine and ultrafine particles of iron ore and silica, [36]. It is estimated that about 40% of this material consists of iron ore, although the percentage depends on the iron content of the deposit from which the ore is extracted, [37]. The sludge has no commercial importance, so it is accumulated and stored in ponds, [38]. Although, there is no direct association with dangerous contaminants, leaching can occur, while maintenance of pond dams is expensive and complicated, with thousands of tons of material often being added daily. The high concentrations of iron can be prejudicial to the environment and in excess can cause human health effects such as damage to the pancreas, liver, and heart, [39].

It is vital to develop alternative technologies for the permanent safe disposal of iron mining waste, in order to avoid disasters such as the one that occurred in November 2015 in Mariana (Minas Gerais State, Brazil). In this accident, sludge derived from the tailings of different stages of the iron mining operation were discharged into the Doce River and were transported for many kilometers downstream, reaching several cities in the States of Minas Gerais and Espírito Santo, before entering the Atlantic Ocean. This event, considered one of Brazil's most serious recent disasters, led to a series of environmental consequences.

Given that these wastes currently have little or no economic worth, innovative strategies need to be developed for their use to produce new technological materials that can provide them with added commercial value, [40], [41]. The systematic use of mine tailings could be an effective way of reducing the extraction of natural resources, minimizing waste generation, and avoiding negative impacts in the environment, [42], [43].

One promising technology for the use of iron mining waste is to recover iron ions and apply them in the synthesis of multifunctional magnetic materials. These consist of combinations of organic and inorganic components whose complementary properties differ from those of the original materials, [44], [45].

Cobalt ferrite ($CoFe_2O_4$) nanoparticles (NPs) is a well-known hard magnetic material with high coercivity and moderate magnetization. The properties of $CoFe_2O_4$ are strongly dependent on factors such as particle size and shape, degree of crystallinity and phase purity. These properties, along with their great physical and chemical stability, make $CoFe_2O_4$ suitable for many applications such as generator, audio, video-tape, medicine, food, cancer treatment and in electronics industry etc. $CoFe_2O_4$ NPs possesses the highest value of absolute magnetostriction co-efficient ($k = - 110 \times 10^{-6}$) among all the known spinel ferrites along with ferromagnetic behavior, [46], [47]. $CoFe_2O_4$ NPs adopt inverse spinel structure in which, all the Co^{2+} ions occupy the B sites, and Fe^{3+} ions are equally distributed between A sites and B sites. $CoFe_2O_4$ NPs are widely being studied owing to their excellent electromagnetic performance, mechanical hardness, moderate saturation magnetization, chemical stability, high electrical resistivity, high permeability, high coercivity and low hysteresis loss which make it a suitable material for making recording devices, and magnetic cards used in computers, [48], and in gas sensors, [49], magneto-optical devices, [50], photocatalyst, [51], magnetic hyperthermia, [52], contrast agents for magnetic resonance imaging, [53], cancer imaging and therapy, [54], targeted drug delivery, [55], theragnostic, [56], ferrofluids, [57], and lithium-ion batteries, [58].

$CoFe_2O_4$ NPs have been successfully proved to be temperature dependent on the grain size distribution. $CoFe_2O_4$ NPs is showed that larger deposition temperature in the synthesis, the grain size of the generated $CoFe_2O_4$ NPs will also increase, [59]. The properties of $CoFe_2O_4$ NPs are different from those of their bulk counterparts. Moreover, the size dependent physicochemical properties of $CoFe_2O_4$ NPs provide a wide range of prospects to the materials researchers for emerging devices, [60]. Usually, actuators and sensors are made by using magnetostrictive materials such as Terfenol-D. As $CoFe_2O_4$ NCs possesses high magnetocrystalline anisotropy constant of (2.71×10^6 J/m), high coercivity (4.3 kOe), high Curie temperature (520°C), and moderate saturation magnetization (80 emu/g), it acts as an excellent alternative material for Terfenol-D, [61]. Further, the synthesis technique, medium in which the reaction takes place, time duration is the key factors which govern the properties of the $CoFe_2O_4$ NPs, [62]. Apart from these factors, addition of dopants also greatly influences the properties. $CoFe_2O_4$ NPs are synthesized using different techniques such as microwave assisted hydrothermal method, [63], solvothermal method, [64], modified citrate gel technique, [65], auto combustion sol-gel technique, [66], micro-emulsion technique, [67], mechanical alloying, [68], normal and reverse micelle technique, co-precipitation method, [69], and microwave-assisted combustion method, [66].

A hybrid magnetic material was synthesized using water with a high content of natural organic matter (NOM) as the organic phase, with commercial iron as an inorganic precursor. Here, it is proposed to use the iron recovered from mine tailings as the inorganic phase of the hybrid and for production of the magnetic part of the ferrite structure. Ferrite has been used previously in a wide range of applications, such as in drug carriers, information storage, nuclear magnetic resonance, treatment of malignant tumors, ceramic pigments, catalysis, and environmental remediation, [70], [71].

Magnetic hybrid materials in which ferrite is the inorganic phase have been employed for the removal of various organic contaminants, [72], [73]. Notable among the latter are nitrophenols, which are found in wastewaters originating from the pharmaceutical, paper, and agricultural sectors, [74], [75]. However, their reduction results in the formation of aminophenol, a less toxic compound that is considered a valuable input in the pharmaceutical and dye industries, among others, and that can also be further degraded by microorganisms, [76].

Other important persistent pollutants are the nanoplastics, which are resistant to biodegradation and present toxic, carcinogenic, and/or mutagenic properties, [77], [78], [79].

The objective of this work was to synthesize a nanocomposite namely $CoFe_2O_4$/NOM with high magnetic properties, using iron ions recovered from iron ore mining tailings. The products were evaluated in terms of their potential for the catalytic reduction of PE, PP, PS and PVC polymers, respectively. The characteristics of the synthesized $CoFe_2O_4$/NOM NCs were assessed using XRD, FTIR, FESEM, HRTEM, and VSM analyses, respectively. The effects of some operational conditions ($CoFe_2O_4$/NOM dose, $CoFe_2O_4$ to NOM ratio, pH, sunligth power, temperature, contact time, aging and reuse of nanocomposite) on the photodegradation yields of PE, PP, PS and PVC polymers were investigated.

2 Materials and Methods

2.1 Synthesis of Ferric Sulfate from Iron Mine Tailings and Acid Extraction from Iron Mine Tailings Sludge

The iron precursors used in the synthesis was derived from different industrial wastes, resulting in a magnetic hybrid material. First, consisting mainly of ferric sulfate, was from iron mine tailings treated by a commercial company, and the resulting hybrid was named iron precursor.

The hybrid material was synthesized according to the method reported previously, [80]. Briefly, $CoCl_2.6H_2O$ (analytical grade) and waste iron salts were dissolved in 150 ml of NOM-rich water. The pH of the solution was progressively adjusted to pH=9.0 with 1 mol/l NaOH. Subsequently, the system was stirred for 30 min and heated at 100ºC to remove water. The materials obtained were rinsed extensively with deionized water and were then dried at 60ºC.

2.2 Production of $CoFe_2O_4$/NOM NCs

The iron precursors were obtained from ferric sulfate from iron mine tailings and acid extraction of iron mine tailings sludge. $CoCl_2.6H_2O$ and $FeCl_3.6H_2O$, which were dissolved in 200 ml of NOM-rich water, using cobalt/iron/NOM proportions of 7.0/13.9/0.024 g/l. The pH of the medium was then adjusted to pH=9.0 with aqueous 1 mol/l NaOH, after which the system was maintained under mechanical stirring for 30 min.

After gel formation, the system was heated at 100°C for 6 h to remove water and obtain a xerogel. The resulting material was washed, dried in an oven at 60°C, and homogenized. For comparative purposes, the $CoFe_2O_4$/NOM NCs hybrid obtained at 25ºC room temperature was calcined at 200, 400, and 800°C in an electric muffle furnace, under an ambient atmosphere, using a heating rate of 10°C/min.

$CoCl_2.6H_2O$ (analytical grade) and waste iron salts were dissolved in 150 ml of NOM-rich water. The pH of the solution was progressively adjusted to pH=9.0 with 1.0 mol/l NaOH. Subsequently, the system was stirred for 30 min and heated at 100°C to remove water. The materials obtained were rinsed extensively with deionized water and were then dried at 60°C.

2.3 Adsorption Mechanisms

The proposed adsorption mechanism for formation of the materials was based on the synthesis method in literature, [81], and the information obtained in the characterization analyses.

In the literature, for this study, the proposed adsorption mechanism was explained as follows: The synthesis of the $CoFe_2O_4$/NOM NC hybrid, was performed at room temperature using NOM, a natural polymer that is able to anchor metal species derived from inorganic precursors, therefore, avoiding use of the expensive and toxic organic solvents that are employed in traditional sol-gel syntheses, [81]. The formation mechanism of $CoFe_2O_4$/NOM nanocomposites according to a sol-gel process, [82], was shown in Fig. 1.

* Fig. **1** can be found in the Appendix section.

The complexing agent used was NOM, so the phenolic, carboxylic and hydroxyl sites present in many of its components could have been involved in the nanoparticle formation. As reported by Tan, [83], carboxylic groups are deprotonated at around pH=4.0, while phenolic hydroxyls are deprotonated at pH=9.0. In this work, the synthesis was performed at pH=9.0, for this reason, the hydrolyzed iron species were present in the cationic form ($FeOH^+$). These ions can be stabilized by the deprotonated groups of NOM ($–COO^-$ and $–O^-$), leading to gelification of the solution and formation of polymeric chains, which after drying form the desired ferrite phase, [84]. During the inorganic precursor poly condensation process, the NOM molecules were randomly dispersed; at the gel point, they became bound to the inorganic network, subsequently remaining in it after the elimination of water. In this way, NOM promotes synthesis of the hybrid and its presence in the structure enhances the adsorptive capacity.

The complexation capacity of NOM is due to the fact that its composition is rich in functional groups (especially carboxyls and phenolic hydroxyls) whose acid-base behavior makes the capacity for complexation of metals dependent on the pH of the medium, [85], [86], [87].

2.4 Characterizations

2.4.1 X-Ray Diffraction (XRD) Analysis

Powder XRD patterns were recorded on a Shimadzu XRD-7000, Japan diffractometer using Cu Kα radiation (λ=1.5418 Å, 40 kV, 40 mA) at a scanning speed of 1º min^{-1} in the 10-80º 2θ range. Raman spectrum data was collected with a Horiba Jobin Yvon-Labram HR UV-Visible NIR (200-1600 nm)

Raman microscope spectrometer, using a laser with λ=512 nm. The spectrum was collected from 10 scans at a resolution of 2 cm^{-1}. The zeta potential was measured with a SurPASS Electrokinetic Analyzer (Austria) with a clamping cell at 300 mbar.

2.4.2 Fourier Transform Infrared Spectroscopy (FTIR) Analysis

The FTIR spectra of samples was recorded using the FT-NIR spectroscope (RAYLEIGH, WQF-510). Experimental were scanned using infrared light and their samples chemical properties were observed in FTIR spectra.

2.4.3 Field Emission Scanning Electron Microscopy (FESEM) Analysis

The morphological features and structure of the synthesized catalyst were investigated by FESEM (FESEM, Hitachi S-4700). FESEM images were used to investigate the composition of the elements present in the synthesized nanocomposite.

2.4.4 High Resolution Transmission Electron Microscopy (HRTEM) Analysis

The size and structure of the $CoFe_2O_4$/NOM NCs samples were identified with HRTEM analysis. The obtained $CoFe_2O_4$/NOM NCs was collected and harvested by centrifugation (8000 rpm, 5 min), washed twice with deionized water and resuspended in ethanol (C_2H_6O) and dripped onto a carbon-coated copper (Cu) TEM grid. Vacuum drying then occurred to the $CoFe_2O_4$/NOM NCs for 24 h at 25ºC room temperature. The dry samples on the Cu grid were viewed and examined by HRTEM analysis recorded in a JEOL JEM 2100F, Japan under 200 kV accelerating voltage.

2.4.5 Value Stream Mapping (VSM) Analysis

In order to explain the magnetic property of $CoFe_2O_4$/NOM NCs, the magnetic hysteresis curve was measured at 25ºC. The hysteresis loop exhibits ferromagnetic behavior with saturation magnetization (Ms) of 2.59 emu/g.

2.4.6 UV-vis Spectra Analysis

UV-vis spectra in the range of 200–800 nm were recorded on a Cary 5000 spectrophotometer from Varian.

2.4.7 Gas Chromatography–Mass Spectrometry (GC-MS)

The experimental samples (PE, PP, PS and PVC polymers) analyzed by gas chromatography–mass spectrometry (GC-MS) and gas chromatograph (GC) (Agilent Technology model 6890N) equipped with a mass selective detector (Agilent 5973 inert MSD). Mass spectra were recorded using a VGTS 250 spectrometer equipped with a capillary SE 52 column (HP5-MS 30 m, 0.25 mm ID, 0.25 µm) at 220°C with an isothermal program for 10 min. The initial oven temperature was kept at 50ºC for 1 min, then raised to 220ºC at 25ºC/min and from 200 to 300ºC at 8ºC/min, and was then maintained for 5.5 min. High purity He(g) was used as the carrier gas at constant flow mode (1.5 ml/min, 45 cm/s linear velocity).

2.5 PE, PP, PS and PVC Nanoplastics Adsorption and Photocatalytic Experiments

Chromatographic analyses of the mixed PE, PP, PS and PVC nanoplastics solution were performed using an Agilent 1100 high performance liquid chromatography (HPLC) system consisting of an automatic injector, a gradient pump, a Hewlett–Packard series 1100 photodiode array detector. C-18 reverse phase HPLC column (Ace 5C18; 25-cm x 4.6-mm, 5 µm, mobile phase: 50/50 (v/v) methanol/organic-free reagent water).

A mixture of water and acetonitrile was used as the mobile phase, at a flow rate of 1 ml/min, with the following elution conditions: 75% acetonitrile for 5 min, linear ramp to 95% acetonitrile in 25 min, return to 75% acetonitrile in 30 min, and constant 75% acetonitrile for another 5 min. The detector was maintained at excitation/emission wavelengths of 260/385 nm up to 20 min, followed by a switch to 290/440 nm for the remainder of the period.

Certified standards of PE, PP, PS and PVC polymers were acquired from Sigma-Aldrich (Supelco brand). Analytical curves were constructed using solutions containing the four nanoplastics (PE, PP, PS and PVC) at concentrations in the range 10–150 µg/l.

The adsorption experiments were carried out in batch processes in amber flasks, at 25°C, using 10 ml of 100 µg/l PE, PP, PS and PVC polymers mixed solution. Masses of 20 mg of mixed PE, PP, PS and PVC polymers were added to the flasks and the systems were kept under agitation at 150 rpm (Model MA 832/1 shaker, Marconi) for predetermined time intervals between 5 and 100 min. The adsorbents were separated from the aqueous media using a neodymium magnet, followed by determination of the PE, PP, PS, and PVC polymers concentrations in the aqueous solution by HPLC. The assays were performed in triplicate, including a control solution prepared without the adsorbent material.

2.6 Catalytic Reduction of PE, PP, PS and PVC NanoplasticPolymers

The procedure for the catalytic reduction of PE, PP, PS and PVC polymers was carried out according to Goyal et al., [88], with modifications. A 25 µl aliquot of 0.036 mol/l PE, PP, PS and PVC polymers mixed solution was mixed with 5 ml of 3.2 mol/1 $NaBH_4$ (sodium borohydride, or sodium tetrahydridoborate also known as sodium tetrahydroborate) solution and stirred for 1 min at room temperature. Then, 10 mg of the catalyst was added to the mixture and the time was recorded until the bright yellow solution became colorless, confirming the reduction of PE, PP, PS and PVC polymers. After completion of the reaction, the catalyst was recovered using an external neodymium magnet, washed with deionized water, dried, and reused.

2.7 Statistical Analysis

ANOVA analysis of variance between experimental data was performed to detect F and P values. The ANOVA test was used to test the differences between dependent and independent groups, [89]. Comparison between the actual variation of the experimental data averages and standard deviation is expressed in terms of F ratio. F is equal (found variation of the date averages/expected variation of the date averages). P reports the significance level, and d.f indicates the number of degrees of freedom. Regression analysis was applied to the experimental data in order to determine the regression coefficient R^2, [90]. The aforementioned test was performed using Microsoft Excel Program.

3 Results and Discussions

3.1 XRD Analysis Results

The XRD analyses (Fig. 2) confirmed formation of the $CoFe_2O_4$ NPs phase in both samples. The most intense peaks observed for $CoFe_2O_4$/NOM NCs were related to the cubic spinel structure (space group Fd-3mZ), in agreement with the Inorganic Crystal Structure Database standard (ICSD card #192031). The absence of other broather diffraction peaks indicated the efficiency of the synthesis route in which cobalt ferrite was obtained without a calcination step, unlike traditional routes such as hydrothermal and solvothermal reactions, the microemulsion method, the vapor phase method, and the sol-gel method itself, which require heat treatment at high temperatures and employ expensive solvents. The results highlight the success of the route proposed in this work for synthesis of the $CoFe_2O_4$/NOM hybrid, which was performed at room temperature using NOM, a natural polymer that is able to anchor metal species derived from inorganic precursors, hence avoiding use of the expensive and toxic organic solvents that are employed in traditional sol-gel syntheses, [81], [86]. The complexation capacity of NOM is due to the fact that its composition is rich in functional groups (especially carboxyls and phenolic hydroxyls) whose acid-base behavior makes the capacity for complexation of metals dependent on the pH of the medium, [85], [87].

According to Tan, [83], carboxylic groups are deprotonated at around pH=4.0, while hydroxyls are deprotonated at pH=9.0. In this work, the synthesis was performed at pH=9.0, at which hydrolyzed iron species are found in the cationic form, $FeOH^+$, [91]. These ions can be stabilized by the deprotonated groups of NOM ($–COO^-$ and $–O^-$), leading to gelification of the solution and formation of polymeric chains, which after drying form the desired ferrite phase. In this way, NOM promotes synthesis of the hybrid and its presence in the structure enhances the adsorptive capacity.

A lower degree of crystallinity of the $CoFe_2O_4$/NOM NC was probably due to the presence of NOM in its structure. When the calcination temperature was increased, the degree of crystallinity increased, resulting in a diffractogram with a less noisy baseline and better-defined peaks, due to the progressive removal of organic matter. According to Pertusatti, [92], NOM degradation begins at about 240ºC and ends near 740ºC. However, in the case of the sample calcined at 800ºC, it is possible that the hybrid structure still contained a residual amount of organic matter, such as aromatic compounds that exhibited high thermal stability.

The iron content in the solution was due to leaching of the $CoFe_2O_4$ by HCl during desorption to release the active sites. However, it was noted that the adsorbent matrix did not suffer any loss of its magnetic properties during the desorption tests. The leaching of iron was advantageous, since it conferred magnetic properties on the $CoFe_2O_4$, hence providing a characteristic highly desirable for efficient catalysts, namely easy separation from the reaction medium, [88], [93].

The infrared spectrum of $CoFe_2O_4$/NOM NC with broad bands in the region 3300–3430 cm^{-1} attributed to the OH groups. A band at around 1626 cm^{-1} could be attributed to of C-C bonds of aromatic groups, and could also be associated with carboxylate groups, [92], [94], [95]. Bands at around 1100 cm^{-1} in the spectra of samples orresponded to stretching of C-O bonds, [96], [97], probably due to the high concentration of this species in the effluent.

* Fig. 2 can be found in the Appendix section.

3.2 FTIR Analysis Results

Fig. 3 was illustrated the infrared spectra of $CoFe_2O_4$/NOM NCs. The spectra showed a broad band at around 3400 cm^{-1}, generally attributed to OH groups indicating the presence of water, and/or carboxylic acids. A band at 1629 cm^{-1} was assigned to aromatic C = C bonds, while a band at 1366 cm^{-1} was ascribed to symmetric stretching of COO^-. These bands are characteristic of NOM, [98].

An absorption band at around 599 cm^{-1} could be attributed to the Fe-O bond, characteristic of ferrites, [99]. These data corroborated the diffractograms, because the bands at 1629 and 1529 cm^{-1} observed in all the spectra revealed the presence of NOM in the structure of the nanocomposite, even in the case of the hybrid calcined at 800ºC.

A band at around 1105 cm^{-1} in the $CoFe_2O_4$/NOM NCs corresponding to stretching of C = O bonds, was indicative of the presence of -COOH, [79], [100], derived from the solution of mining waste used in the synthesis, which was mainly composed of ferric sulfate. The spectrum of $CoFe_2O_4$/NOM NCs showed a band at around 990 cm^{-1} that could be attributed to the Fe-O bonds of silicate impurities derived from the ferrites, [99], originated from tailing's sludge which the iron ions were extracted, **[**101].

* Fig. 3 can be found in the Appendix section.

3.3 Surface Area (S_{BET}) Determinations

The specific surface areas, pore volumes, and pore sizes of the $CoFe_2O_4$/NOM NC studied here are provided in **Table 1.** The samples showed high surface areas of 357.0 m^2/g, while iron oxides recovered from acid mine drainage presented a surface area of 163 m^2/g, after calcination at 300°C, **[**102]. The surface area of $CoFe_2O_4$ NP was measured to be 41.3 m^2/g, [103]. A high surface area is a desirable feature of an adsorbent, because it improves performance in the removal of pollutants. The results showed that the surface areas of the calcined $CoFe_2O_4$ hybrids were smaller compared to that of the $CoFe_2O_4$/NOM NC, which could have been due to the different amounts of the NOM polymer. According to Faraji et al., [104], polymers or surfactants prevent particle agglomeration, due to the effects of electrostatic and/or steric repulsion.

* **Table 1** can be found in the Appendix section.

Zhang et al., [105], obtained $CoFe_2O_4$ with a surface area of 101 m^2/g by a chemical co-precipitation method. Culita et al., [99], synthesized $CoFe_2O_4$ with a surface area of 93.7 m^2/g using CTAB as surfactant and heat treatment at 400ºC. Khan et al., [106], reported the synthesis of a $CoFe_2O_4$ composite with surface area of 335 m^2/g by the sol-gel route, employing egg albumen and calcination at 500ºC. The surface areas of the hybrids obtained in the present work compared well with those reported previously, highlighting the technological potential of the proposed eco-friendly synthesis route, especially in the case of the HbAmb hybrid obtained without heat treatment, which had the highest specific surface area.

In the studies performed by Liu et al., [107], Klempova et al., [108], and Paik et al., [109], and Chen et al., [110], different light sources (320-780 nm) resulted in noticeable fissures on the PS surface, accompanied by a smoother texture, confirming the structural damage under simulated photolytic conditions with $CoFe_2O_4$. No significant changes in PS surface morphology were observed suggesting that mechanical agitation alone did not influence PS morphology. In the case of PVC, the original surface of MPs displayed intact and regular shapes.

3.4 FESEM Analysis Results

The FESEM micrographs of the $CoFe_2O_4$/NOM NCs hybrid particles was shown in Fig. 4. It is possible to observe agglomerates of irregularly shaped particles and rough surfaces, which confirmed the high surface areas of the materials. The magnified FESEM image revealed that the product had a unique double-shelled structure, and the thickness of the $CoFe_2O_4$ cubic shell is measured to be 13 nm. It was observed from the micrograph of sample annealed at 600°C, the grain size of the $CoFe_2O_4$/NOM NC is in the range of 26 nm to 36 nm. The sample which was annealed at 800ºC, the grain size is in the range of 60 nm to 127 nm.

* Fig. 4 can be found in the Appendix section.

3.5 HRTEM Analysis Results

The HRTEM image of $CoFe_2O_4$/NOM NCs was illustrated to confirmed the formation of nanostructures (Fig. 5). The results of HRTEM indicate that $CoFe_2O_4$/NOM NCs are solidly bonded between the CoFe alloy and $CoFe_2O_4$ with a distinct interface, and there exists 002 plane of graphitic carbon (interplanar spacing d = 0.358 nm)

* Fig. 5 can be found in the Appendix section.

3.6 Magnetic Analysis

Fig. 6 shows the magnetization curves as a function of the magnetic field up to ± 90 kOe, measured at temperatures of – 269.15ºC and 26.85ºC. In the inset, magnifications of the curves are shown for better visualization of the coercive field and the remaining magnetization. In the curves acquired at 26.85ºC room temperature, the $CoFe_2O_4$/NOM NCs hybrid sample showed characteristic behavior of soft magnetic material, with low coercive field of 360 Oe and remaining magnetization of 3.54 emu/g (Fig. 6). The $CoFe_2O_4$/NOM NCs sample showed the behavior of a superparamagnetic material, since it had no coercivity or remaining magnetization, presenting a null liquid magnetic moment when there was no applied field, [111], [112**]**.

* Fig. 6 can be found in the Appendix section.

At – 269.15ºC, a change in the magnetic behavior of $CoFe_2O_4$/NOM NCs was observed, with the appearance of a hysteresis loop accompanied by increases of coercivity to 12.5 KOe and remaining magnetization to 11.9 emu/g (Fig. 6). In relation to this increase, it is possible that freezing of the magnetic moments occurred when the samples were cooled, consequently increasing the magnetizations and coercive fields. The maximum magnetizations measured at 26.85ºC room temperature for a field of up to ± 90 kOe were 18 emu/g for $CoFe_2O_4$/NOM NCs hybrid sample (Fig. 6). It is evident from Fig. 6 that the maximum applied field was not sufficient to saturate the sample.

The results indicated that the wastes could be used in the elaboration of new materials, replacing traditional analytical grade reagents, and that the hybrids had an excellent magnetic response when submitted to an external magnetic field. In addition, the synthesis was successful at 26.85ºC room temperature and using a natural solvent, in contrast to traditional syntheses using highly toxic solvents that do not degrade easily and can remain in the environment for years, such as cetyltrimethylammonium bromide (cetrimonium bromide, CTAB), polyacrylic acid (PAA), polyethylene glycol (PEG), and others, **[**113].

3.7 Evaluation of Catalytic Activity

The catalytic reduction of PE, PP, PS and PVC polymers using sodium borohydride (also known as sodium tetrahydridoborate and sodium tetrahydroborate, $NaBH_4$) as reducing agent is one of the most widely studied reaction models for the conversion of aromatic nitro compounds to aromatic amines, [114], [115], [116]. The UV–vis spectra analysis was examined for the reduction of PE, PP, PS and PVC nanoplastics with the $CoFe_2O_4$/NOM NCs matrices as catalysts. Before addition, a band at 400 nm corresponded to $CoFe_2O_4$/NOM NCs formed by the addition of $NaBH_4$ solution, [117].

After addition of the magnetic catalysts, the solution changed color from yellow to colorless within seconds. The color modification was associated with the disappearance of the band at 400 nm and the appearance of a band at around 296 nm, due to the production of PE, PP, PS and PVC polymers.

The factors influencing the catalytic activities of these magnetic materials include the distribution of the metal ions between the tetrahedral and octahedral ferrite sites, as well as the surface area of the material. With 10 mg/l $CoFe_2O_4$/NOM NCs hybrid materials 89.2% and 99.9% removal rates were detected after 30 min for removal rates of PE, PP, PS and PVC polymers demonstrating their excellent performance as catalyst compared to the other catalyst (According to **Table 1 in Subsection 3.3**). These results could be explained by the presence of Co^{2+} and Fe^{3+} ions at the octahedral ferrite sites, [118], which were more exposed and had greater interaction with the reactant molecules, [119], [120]. In addition, the perfect catalytic activity of $CoFe_2O_4$/NOM NCs was consistent with its greater surface area.

The reduction of PE, PP, PS and PVC polymers using a catalyst consisting of $CuFe_2O_4$ NPs was achieved in 50 min, [121], while it was found that the same reduction required a time of 130 min using a magnetic Co-carbon composite as catalyst, [122]. Therefore, it was evident that the hybrids synthesized in the present work, using iron precursors extracted from mining wastes, showed catalytic activities similar to or greater than those reported in the studies mentioned above.

3.8 Adsorption Experiments of PE, PP, PS and PVC Polymers

PE, PP, PS and PVC polymers removal assays were performed to show the effectivity of the $CoFe_2O_4$/NOM NCs hybrids. Table 2 exhibits the adsorption percentages obtained for the nanoplastics namely PE, PP, PS and PVC present in mixed solution, using 10 mg/l $CoFe_2O_4$/NOM NCs hybrid materials. It can be seen that the nanoplastic yields varied between 99.20% and 99.90% for the aforementioned polymers at 1000 mg/l initial concentration in 30 min, at 1000 demonstrating that $CoFe_2O_4$/NOM NC could provide effective remediation of media contaminated with PE, PP, PS and PVC polymers (Table 2).

* Table 2 can be found in the Appendix section.

The $CoFe_2O_4$/NOM NCs hybrid showed a perfect performance, probably due to the presence of double bonds derived not only from the NOM, but also from the sulfate structures, which interacted with the aromatic rings of the nanoplastics. Such interactions, known as π-π, represent one of the main mechanisms of adsorption of nanoplastics, [80]. Furthermore, the removal percentages were consistent with the different surface areas (S_{BET}) of the materials, which were in the order $CoFe_2O_4$/NOM NCs.

Considering previously reported studies involving the removal of PE, PP, PS and PVC polymers, it was evident that the materials employed in the present work provided superior performance, evidencing the multifunctionality of the magnetic hybrids. For example, Costa et al., [77], employed mesoporous Si–MCM–41 to remove the nanoplastics (PE, PP, PS) from aqueous media, achieving adsorption percentages of 90.43%, 91.2%, and 92.98%, respectively, in 60 min. Coconut waste (CW) and orange waste (OW), as well as their biochars (BCW and BOW), were studied by de Jesus et al., [78], as adsorbents for the removal of nanoplastics from water. Adsorption tests using a mixed solution of PP, PS, PVC and PET showed removal percentages of 80–83% (CW), 79–83% (BCW), 60–74% (OW), and 78–84% (BOW), in 120–180 min. Zeledón-Toruño et al., [123], reported removal values of approximately 70%, in 120 min, for PE and PP, using immature coal (leonardite).

3.9 Effects of Operational Conditions on Removals of PE, PP, PS and PVC Polymers

3.9.1 Effect of Initial pH

In this step of this study, the effects of increasing pH levels on the removal efficiencies of four types of polymers namely PE, PP, PS and PVC was investigated under individual concentration of 1000 mg/l at a $CoFe_2O_4$/NOM NCs concentration of 10 mg/l. The removal yields at all types of polymers elevated with an increase in time until it reached maximum yield at the optimal time of 30 min at pH= 7.0. The maximum polymer yields were around 99.90% and 99.20%. A substantial reduction in all types of microplastics was achieved as the pH was decreased from 7.0 to 4.0, with efficiencies ranging from 99% to 59% (Table 3). PE, PP, PS and PVC polymer removal efficiencies was around 45%-55% at pH ranges between 2.0-3.0 (Table 3). At high pH ratios the yiels of all polymers decreased to around 40%. The removal of polymers was found to be efficient at neutral pH althoug have hydrophobic properties, [124], [125]. The polymer yields increased as the pH values was increased from acidic to neutral conditions. The contribution of pH on the polymer yields was found to be significant up to a pH of 8.0 (R^2 = 0.99, F = 1.03, p = 0.001). Therefore, the correlation between polymer removal efficiencies and alkaline pH values were not foud to be significant (R^2 = 0.32, F = 14.34, p = 0.001).

* Table 3 can be found in the Appendix section.

Iron ions in the nanocomposite showed more solubility at low pH, forming $Fe(OH)_2$, whereas at neutral pH, they tend to form $Fe(OH)_3$, which is less soluble and this enhance the polymer yields, [126]. The pH also affects the charge and size of the metal hydroxide flocs and the polymers. For example, at low pH, the flocs are smaller and carry a more positive charge, which can not attract negatively charged particles like polymers. Conversely, at meutral pH, the flocs are larger and bear a more negative charge, thereby attracting positively charged microplastics like polymers, [127].

Indeed, pH of wastewater is a critical determinant that influences the efficiency and mechanism of pollutant removal during the oxidation. For instance, pH can alter the speciation and hydrophobicity of microplastics in water. Microplastics can exhibit varying surface charges depending on the type of polymers and the initial pH. Polymers constituted from carbon, hydrogen, and oxygen atoms. The oxygen atom in polymers tends to form hydrogen bonds with water molecules, rendering polymers more hydrophilic and thereby facilitating a higher rate of removal at different pH levels, [128]. The benzene ring can create polar regions on the polymer chain, making less hydrophilic polymers.

3.9.2 Effect of Increasing Doses of $CoFe_2O_4$/NOM NC on Photooxidation Rates of Polymers

Experiments were conducted at a pH of 7.0 and a room temperature of 26°C for 30 min. The $CoFe_2O_4$ to NOM ratio in the $CoFe_2O_4$/NOM NCs was 2.1%. As the $CoFe_2O_4$/NOM NCs concentration increased from 0.2 to 10 mg/l, the PE, PP, PS and PVC nanoplastics photodegradation yields increased from 79%-80% to 99.20%-99.90%. Futher increase of $CoFe_2O_4$/NOM NC to 20 and 30 mg/l the polymer yields decreased to around 80%- 87%, (Table 4). The highest PE, PP, PS and PVC polymers photodegradation yields were observed at a $CoFe_2O_4$/NOM NCs concentration of 10 mg/l. Further increasing the $CoFe_2O_4$/NOM NCs concentration to 20 and 30 mg/l resulted a decrease in polymer photodegradation yields. This reduction can be attributed to competitive photon absorption, where a smaller amount of energy is absorbed by the $CoFe_2O_4$/NOM NCs concentration. Consequently, lower photooxidation yields were observed due to competition for sunlight photons among multiple metabolites, [129]. Liu et al., [107], and Bigger et al., [130], reported photodegradation yields of 87% and 90% for polymers using TiO_2/GO/$CuFe_2O_4$ NCs, which were lower than the yields obtained in our study after 1 h of photooxidation with a $CoFe_2O_4$/NOM NCs concentration of 15 mg/l. The polymer yields increased as the $CoFe_2O_4$/NOM NC concentration was increased from 0.2 mg/l to 10 mg/l. The contribution of nanocomposite concentration on the polymer yields was found to be significant up to 2a nanocomposite concentration of 20 mg/l (R^2 = 0.99, F = 1.02, p = 0.001). Therefore, the correlation between polymer removal efficiencies and high $CoFe_2O_4$/NOM NC levels were foud to be not significant (R^2 = 0.30, F = 15.09, p = 0.001).

* Table 4 can be found in the Appendix section.

3.9.3 Effect of $CoFe_2O_4$ to NOM Ratio in $CoFe_2O_4$/NOM NCs

The experimental conditions were set as follows: The $CoFe_2O_4$ to NOM ratios were adjusted between 2%, 4.2%, 5% and 6% within the 10 mg/l $CoFe_2O_4$/NOM NCs, at a contact time of 30 min, a pH of 7.0, and a temperature of 25°C. When the $CoFe_2O_4$ to NOM ratio in the $CoFe_2O_4$/NOM NCs was increased from 2% to 4.2%, the removal efficiencies of PE, PP, PS and PVC polymers improved from 80% to 99.20% and 99.90 (Table 5). However, further increasing of this ratio to 5% and 6% resulted in a slight decrease in photodegradation yields. Specifically, PE, PP, PS and PVC polymers removal efficiencies decreased to 78%-82%, and 69%-74%, respectively (Table 5). This decline in efficiency can be attributed to the excessive $CoFe_2O_4$ content, which may quench electrons and consequently reduce the overall photodegradation yields. The contribution of $CoFe_2O_4$ to NOM ratio on polymer yields was found to be significant up to a ratio of 5% and 6% (R^2 = 0.99, F = 1.025, p = 0.001). Therefore, the correlation between polymer removal efficiencies and high $CoFe_2O_4$ to NOM ratios were found to be not significant (R^2 = 0.37, F = 14.99, p = 0.001).

* Table 5 can be found in the Appendix section.

3.9.4 Effect of Sunlight Power on Photooxidation Rates of Polymers

The optimal operational conditions for this study included 10 mg/l $CoFe_2O_4$/NOM NC dosage, a $CoFe_2O_4$ to NOM ratio of 4.2% within 10 mg/l $CoFe_2O_4$/NOM NC concentration at a contact time of 20 min, at pH of 7.0, and varying sunlight powers of 20, 30, 40 and 60 W/m^2, at a temperature of 25°C. In this step of this study, the effects of increasing sunlight powers on the removal efficiencies of PE, PP, PS and PVC polymers were evaluated. As presented in Table 6, the maximum photodegradation efficiencies of all polymers was detected at between 99.20 and 99.90%, at a sunlight power of 30 W/m^2. Increasing the UV power to 40 and 60 W/m^2 resulted in a slight decrease in polymer yields. The polymer yields reduced to around 78-82% and 69-74%, respectively. These results suggest that increasing of sunlight power to a certain level increase the yields whereas after this limit the polymer efficiencies photodegradation rates of PE, PP, PS and PVC polymers was not influenced. This phenomenon could be attributed to the potential influence of thermoinduced activation, which might alter the degradation mechanism. The contribution of sunlight power on the polymer yields was found to be significant up to power of 40 W/m^2 (R^2 = 0.99, F = 1.027, p = 0.001). Therefore, the correlation between polymer removal efficiencies and high sun light powers were found to be not significant (R^2 = 0.36, F = 15.12, p = 0.001).

* Table 6 can be found in the Appendix section.

It is known that both thermooxidation and photooxidation of these microplastics involve similar chemical mechanisms, but with differing effects on the degradation of their functional properties. The lack of further acceleration in photodegradation with higher irradiance aligns with findings by Philippart et al., [131]. It can be noted that the polymer degradation increased linearly as the light irradiance increased from of 20 to 30 W/m^2. According to Therias et al., [132], the degradation rate of organic compounds obeys a power law equation in relation to incident irradiance in Eq. (1), [133]:

$$Rate = K_{app} I^{\beta} \quad (1)$$

where; β is related to the efficiency of electron-hole formation, trapping and recombination at the catalyst surface, K_{app} is the apparent reaction rate constant, and I is the incident irradiance.

It is assumed that the photon harvesting is efficient, the electron-hole pairs formed are consumed by the chemical process on surface of the catalyst and the recombination process of electron-hole pairs is considered to be negligible on the catalyst surface, [134], [135]. The K_{app} value under the experimental conditions is 2.99 mol /W.h (data not shown).

In the studies performed by Fairbrother, et al., [136], Bardi et al., [137], and Zhu et al., [138], after 72 h of illumination, a significantly enhanced peak appeared on the UV-vis curve, with a shift in position, indicating a mild degradation of PS followed by pronounced depolymerization process. Under weak UV 447 conditions, the absorbance at 194 nm and 272 nm increased over time. This displayed an overall enhancing trend, but the maximum absorbance reached only 0.37. This comparison demonstrated that UVA enhanced the depolymerization of PS with a relatively slow pace. The overall absorbance of PS initially decreased and then increased with minor fluctuations, suggesting that mechanical stirring could induce slight aging of PS in dark conditions. For PVC, two absorption peaks were observed around 192 nm and 270 nm. Upon exposure to UVC conditions, the absorbance at both peaks increased with prolonged illumination, reaching a maximum after 72 h. This manifested that PVC primarily undergoes depolymerization under UVC irradiation. Similarly, UVA had a less noticeable impact on the absorbance of PVC filtrate in the first 24 h, reaching an absorbance of 0.32 after 72 h of irradiation. These findings indicated that PVC experienced depolymerization under these light conditions, although to a lesser degree compared to UVC.

3.9.5 Effect of Temperature on Photooxidation Rates for PE, PP, PS and PVC Polymers

For maximum photooxidation yields of PE, PP, PS and PVC the optimum operational conditions were as follows: 10 mg/l $CoFe_2O_4$/NOM NC dosage, a $CoFe_2O_4$ to NOM ratio of 4.2% within 10 mg/l $CoFe_2O_4$/NOM NC, a contact time of 30 min, at pH of 7.0, and a sunlight power of 30 W/m^2. In order to detect the effects of increasing temperature on the removal efficiencies of PE, PP, PS and PVC the temperature were increased from 20 to 30°C and to 40°C. As presented in Table 7, increasing of temperature from 20 to 30°C resulted in the highest photooxidation efficiencies, However, further increasing the temperature to 40°C led to a slight decrease in yields for all polymers (Table 7). The highest photooxidation efficiencies for all polymers were observed at 30°C, achieving removal rates of 99.20% and 99.90%. The contribution of temperature on the polymer yields was found to be significant up to a temperature of 40°C (R^2 = 0.99, F = 1.022, p = 0.001). Therefore, the correlation between polymer removal efficiencies and high temperatures were found to be not significant (R^2 = 0.38, F = 15.82, p = 0.001).

* Table **7** can be found in the Appendix section.

As temperature increases, the molecular weight and ultimate mechanical properties of the compounds decrease, while carbonyl groups increase during photodegradation. Photooxidation kinetics generally improves with temperature, as higher temperatures enhance the rate of the oxidation reaction. However, $CoFe_2O_4$ NPs can retard the diffusion of iron ions and oxygen atoms, leading to a slight reduction in oxidation rates at elevated temperatures. At higher temperatures, increased diffusion rates can lead to an accelerated oxidation rate, but this effect reaches a dynamic equilibrium at around 40°C. During isothermal holding at this temperature, both the promotion and inhibition effects on ion diffusion balance out, resulting in a slower decrease in the oxidation rate. It is also important to consider that elevated temperatures can lead to heterogeneous degradation due to diffusion-limited oxidation, causing a noticeable decrease in the oxidation rate over time. The optimal temperature for photooxidation yields was found to be 30°C, where the promotion effect of temperature on ion diffusion is most beneficial, leading to higher oxidation rates. As the temperature was increased from 20 to 30ºC the number of active centers elevated with rising temperature, [136], or simply the explanation is a increase of the kinetic rate.

3.9.6 Effect of Aging on the Photodegradation Capacity of Polymers

In order to detect the effect of aging procedure on microplastic yields. The Brunauer–Emmett–Teller (BET) surface area of treated and non-treated polymer samples were investigated, [139]. The surface area of non treated polymer samples were recorded as 169 and 198 cm^2/g, while the surface area of the aged samples were measured between 429 and 522 cm^2/g (Table 8). Compared to literature, the aging procedure was similar in technique and time, the growing in surface area indicated that aging improved the photodegradation yields of all polymers studied (Table 8).

* Table 8 can be found in the Appendix section.

Aged $CoFe_2O_4$/NOM NCs adsorbs more PE, PP, PS, PVC polymers. Adsorption is the main removal mechanism as no biodegradation activity was observed in the photocatalytic process. The aging increases the surface area of nanocomposites, making the surface rougher, by increasing the surface to volume ratio and increase the adssorption affinity to polymers, [140]. With aging, oxidation occurs with oxygen-containing functional groups (carbonyl, hydroxyl, ketone and ester). This increases the polarity of nanocomposites which may increase the sorption of pollutans. Also, the formation of hydrogen-bonds among oxygen-containing functional groups can cause more sorption by aged nanocomposites, [141], [142]. By choosing the optimum nanocomposite concentration, and the other operational conditional parameters maximum polymer yields was obtained. The contribution of aging on polymer yields was found to be significant at aging surfaces (R^2 = 0.99, F = 1.023, p = 0.001). Therefore, the correlation between polymer removal efficiencies and not aging surfaces were found to be not significant (R^2 = 0.32, F = 14.09, p = 0.001).

Wang et al., [143], found that photoaging altered the molecular weight and aromaticity of PE, PVC, PS and PP microplastics. Therefore, extensive presence of cracks in aged microplastics facilitates the formation of dissoved organic carbons and affect positively the photodegradation of microplastics.

Wu et al., [144], and Zhou et al., [145], found a significant effect of photoaging time on the surface chemical changes of microplastics, suggesting that aging of microplastics favors the formation of surface carbonyl groups, forming *e.g.,* ketones, esters, carboxylates, and hydroxyl groups on the surface of aged polymers. As mentioned above, it can be inferred that aged microplutants might have a higher adsorption capacity for inorganic/organic contaminants due to the enhanced hydrophilicity and electronegativity from the increase of oxygen containing functional groups.

3.9.7 Reusability of $CoFe_2O_4$/NOM NC

In order to explore the reuse capacities of the $CoFe_2O_4$/NOM catalyst, ten catalytic cycles were performed. The results (Table 9) showed that after the first cycle, the conversion of 1000 mg/l PE, PP, PS and PVC polymers with 10 mg photooxidation time /l $CoFe_2O_4$/NOM NCs exhibited the same yields after 30 min. 99.20%-99.90% reductions were achieved in all cycles for PE, PP, PS and PVC polymers, respectively, during 10 cycles. Furthermore, the analysis of the iron contents in the solutions after catalytic reduction, exhibited no significant amount of iron in the analyte. Hence, there was no leaching of iron ions from nanocomposite matrices, indicating their good chemical stability and a high degree of purity obtained.

* Table 9 can be found in the Appendix section.

3.9.8 Photodegradation Kinetic of PE, PP, PS and PVC Polymers

Pseudo-first-order kinetic fits were performed in oder to detrmine the photodegradation kinetic constants on four polymers namely PE, PP, PS and PVC. Fig. 7 shows that the rate constant k for the photodegradation of PE, PVC, PS and PP with pseudo first order kinetic rate constants of 0.0985 1/h, 0.0984, 0.0983 and 0.09801/h which were ~ half times higher that for the photodegradation of polyethylene plastic with a rate constant of 0.0489 1/h, [146].

* Fig. 7 can be found in the Appendix section.

Our results confirm that optimal conditions yielded the highest removal efficiencies for PE, PP, PS and PVC microplastics, and they also underscore the biocompatibility of our proposed system. Our findings reveal that the negatively charged nature of polymers enables the formation of heteroaggregates with positively charged $CoFe_2O_4$/NOM. Our research demonstrated the remarkable reusability and stability of the $CoFe_2O_4$/NOM nanocomposite owing to its magnetite properties. The primary objective of this research was to engineer a magnetic, recoverable nano-adsorbent derived from wastes This approach not only contributes to cost reduction in the use of magnetic adsorbents but also streamlines the photodegradation process, reduces nanocomposite consumption, and holds promise for practical applications in enhancing micro/nano plastics removals. Results revealed that PVC and although PS exhibited more pronounced physicochemical changes than PP and PE during photoaging, due to the dichlorination of PVC and the benzene ring of PS similar removal yields was detected for all microplastics.

4 Conclusions

New magnetic hybrids were successfully produced from iron ore mining waste using an eco-friendly synthesis route, providing the waste with a useful final destination and economic value. The synthesized nanomaterials were versatile and could be employed as both catalysts and adsorbents. The produced catalyst, is able to catalytically reduce PE, PP, PS and PVC polymers in very short time periods and in consecutive cycles of reuse, with excellent conversion rates. $CoFe_2O_4$/NOM NC hybrids were effective for the removal of nanoplastics (PE, PP, PS and PVC polymers) from mixed solution. The characteristics of the synthesized $CoFe_2O_4$/NOM NCs were assessed using XRD, FTIR, FESEM, HRTEM, and VSM analyses, respectively.

In our study was employed a lower dosage of $CoFe_2O_4$/NOM NCs (10 mg/l) and achieved high PE, PP, PS and PVC removal efficiencies within a shorter time compared to other studies. An important advantage of the $CoFe_2O_4$/NOM NCs is its excellent regeneration capability, allowing it to be reused for multiple cycles of photodegradation without significant loss of efficacy. Regeneration techniques such as pH adjustment desorption agents or thermal treatments were not necessary in our study, as the nanocomposite could be easily separated using a simple magnet. This eliminates additional costs associated with separation and enhances the economic and environmental sustainability of the $CoFe_2O_4$/NOM NCs for wastewater treatment applications.

Given the promising results of the $CoFe_2O_4$/NOM NCs in wastewater for PE, PP, PS and PVC treatments, future research should focus on exploring its potential for remediating other pollutants and further optimizing its use in environmental remediation processes. Notably, there was no sludge production during the photocatalytic treatment of PE, PP, PS and PVC containing these were ultimately photodegraded to CO_2 and water with yields of 99.20% and 99.90%.

The proposed process offers an environmentally friendly, economical, and effective new methodology for the production of nanocomposites from the wastes, generating commercial interest and, most importantly, helping to minimize environmental damage and pollution.

Acknowledgement:
Experimental analyzes in this study were performed at the Laboratories of the Canada Research Center, Ottawa, Canada. The authors would like to thank this body for providing financial support.

References:
[1] R. Miandad, M. Barakat, A.S. Aburiazaiza, M. Rehan, I. Ismail, A. Nizami, Effect of Plastic Waste Types on Pyrolysis Liquid Oil. *International Biodeterioration and Biodegradation*, Vol.119, 2017, pp. 239–252.
[2] A. Kumar, S. Samadder, N. Kumar, C. Singh, Estimation of the Generation Rate of Different Types of Plastic Wastes and Possible Revenue Recovery from Informal Recycling, *Waste Management*, Vol.79, 2018, pp. 781–790.
[3] R. Geyer, J.R. Jambeck, K.L. Law, Production, Use, and Fate of All Plastics Ever Made, *Science Advances*, Vol.3, No.7, 2017, pp. 1-5, e1700782.
[4] M. Gahleitner, C. Paulik, *Polypropylene*, *in Ullmann's Encyclopedia of Industrial Chemistry*, Weinheim: Wiley-VCH, Germany, pp. 1–44, 2014.
[5] S. Wang, S., J.K. Muiruri, X.Y.D. Soo, S. Liu, W. Thitsartarn, B.H. Tan, A. Suwardi, Z. Li, Q. Zhu, X.J. Loh, Bio-Polypropylene and Polypropylene-based Biocomposites: Solutions for a Sustainable Future, *Chemistry: An Asian Journal*. Vol.18, No.2, 2023, e202200972.
[6] G. George, S.M. Simon, V.P. Prakashan, M.S. Sajna, M. Faisal, R. Wilson, A. Chandran, P.R. Biju, C. Joseph, N.V. Unnikrishnan, Green and Facile Approach to Prepare Polypropylene/in Situ Reduced Graphene Oxide Nanocomposites with Excellent Electromagnetic Interference Shielding Properties, *RSC Advances*, Vol.8, 2018, 30412.
[7] A. Ameli, M. Nofar, S. Wang, C.B. Park, Lightweight Polypropylene/Stainless-Steel Fiber Composite Foams with Low Percolation for Efficient Electromagnetic Interference Shielding, *ACS Applied Materials & Interfaces*, Vol.6, 2014, pp. 11091–11100.
[8] A., Ameli, P.U. Jung, C.B. Park, Electrical Properties and Electromagnetic Interference Shielding Effectiveness of Polypropylene / Carbon Fiber Composite Foams, *Carbon*, Vol.60, 2013, pp. 379–391.
[9] M.S. Hong, W.K. Choi, K.H. An, S.J. Kang, S.J. Park, Y.S. Lee, B.J. Kim, Electromagnetic Interference Shielding Behaviors of Carbon Fibers-Reinforced Polypropylene Matrix Composites: II. Effects of Filler Length Control, *Journal of Industrial and Engineering Chemistry*, Vol.20, 2014, pp. 3901–3904.
[10] J. Scheirs, D. Priddy, *Modern Styrenic Polymers: Polystyrenes and Styrenic Copolymers*, John Wiley & Sons. p. 3, 2003.
[11] G.T. Carroll, M.E. Sojka, X. Lei, N.J. Turro, J.T. Koberstein, Photoactive Additives for Cross-Linking Polymer Films: Inhibition of Dewetting in Thin Polymer Films, *Langmuir*, Vol.22, No.18, 2006, pp. 7748–7754.
[12] B.G. Kwon, K. Saido, K. Koizumi, H. Sato, N. Ogawa, S.-Y. Chung, T. Kusui, Y. Kodera, K. Kogure, Regional Distribution of Styrene Analogues Generated from Polystyrene Degradation Along the Coastlines of the North-East Pacific Ocean and Hawaii, *Environmental Pollution*, Vol.188, 2014, pp. 45–49.
[13] Y. Yang, J. Yang, W.M. Wu, J. Zhao, Y. Song, L. Gao, R. Yang, L. Jiang, Biodegradation and

Mineralization of Polystyrene by Plastic-Eating Mealworms: Part 1. Chemical and Physical Characterization and Isotopic Tests, *Environmental Science & Technology*. Vol.49, No.20, 2015, pp. 12080–12086.

[14] Z. Chen, L. Gao, Synthesis and Magnetic Properties of $CoFe_2O_4$ Nanoparticles by Using PEG as Surfactant Additive, *Materials Science and Engineering: B*, Vol.141, No.1–2, 2007, pp. 82-86.

[15] C. Leng, J. Wei, Z. Liu, J. Shi, Influence of Imidazolium-based Ionic Liquids on the Performance of Polyaniline–$CoFe_2O_4$ Nanocomposites, *Journal of Alloys and Compounds*, Vol.509, No.6, 2011, pp. 3052-3056.

[16] P. Martins, C Caparros, R. Gonçalves, P.M. Martins, M. Benelmekki, G. Botelho, S. Lanceros-Mendez, Role of Nanoparticle Surface Charge on the Nucleation of the Electroactive β-poly (vinylidene fluoride) Nanocomposites for Sensor and Actuator Applications, *The Journal of Physical Chemistry C*, Vol.116, No.29, 2012, pp. 15790-15794.

[17] M. Sivakumar, S. Kanagesan, R. Suresh Babu, S. Jesurani, R. Velmurugan, C. Thirupathi, T. Kalaivani, Synthesis of $CoFe_2O_4$ Powder via PVA Assisted Sol–Gel Process, *Journal of Materials Science: Materials in Electronics*, Vol.23, 2012, pp. 1045-1049.

[18] A.B. Salunkhe, V.M. Khot, N.D. Thorat, M.R. Phadatare, C.I. Sathish, D.S. Dhawale, S.H. Pawar, Polyvinyl Alcohol Functionalized Cobalt Ferrite Nanoparticles for Biomedical Applications, *Applied Surface Science*, Vol.264, 2013, pp. 598-604.

[19] M. Zhong, P. Fei, X. Fu, Z. Lei, B. Su, Synthesis of PS–$CoFe_2O_4$ Composite Nanomaterial with Improved Magnetic Properties by a One-Step Solvothermal Method, *Industrial & Engineering Chemistry Research*, Vol.52, 2013, pp. 8230–8235.

[20] M. Vadivela, R. Ramesh Babua, K. Ramamurthi, M. Arivanandhan, Enhanced Dielectric and Magnetic Properties of Polystyrene Added $CoFe_2O_4$ Magnetic Nanoparticles, *Journal of Physics and Chemistry of Solids*, Vol.102, 2017, pp. 1-11.

[21] W.W. Titow, *PVC Technology*, Springer. Inc., pp. 6-15, ISBN 978-0-85334-249-6, 1984.

[22] G. Grause, S. Hirahashi, H. Toyoda, T. Kameda, T. Yoshioka, Solubility Parameters for Determining Optimal Solvents for Separating PVC from PVC-Coated PET Fibers, *Journal of Material Cycles and Waste Management,* Vol.19, No.2, 2017, pp. 612–622.

[23] T. Yoshioka, T. Kameda, M. Ieshige, A. Okuwaki, Dechlorination Behaviour of Flexible Poly(vinyl chloride) in NaOH/EG Solution, *Polymer Degradation and Stability*, Vol.93, 2008, pp. 1822–1825.

[24] B. Lv, G. Zhao, N. Li, C. Liang, Dechlorination and Oxidation for Waste Poly(vinylidene chloride) by Hydrothermal Catalytic Oxidation on Pd/AC Catalyst, *Polymer Degradation and Stability*, Vol.94, 2009, pp. 1047–1052.

[25] T. Li, P. Zhao, M. Lei, Z. Li, Understanding Hydrothermal Dechlorination of PVC by Focusing on the Operating Conditions and Hydrochar Characteristics. *Applied Sciences*, Vol.7, No.3, 2017, 256, pp. 1-9.

[26] A. Castro, D. Soares, C. Vilarinho, F. Castro, Kinetics of Thermal De-Chlorination of PVC under Pyrolytic Conditions, *Waste Management*, Vol.32, No.5, 2012, pp. 847–851.

[27] Q. Cao, G. Yuan, L. Yin, D. Chen, P. He, H. Wang, Morphological Characteristics of Polyvinyl Chloride (PVC) Dechlorination During Pyrolysis Process: Influence of PVC Content and Heating Rate, *Waste Management*, Vol.58, 2016, pp. 241–249.

[28] Y. Tang, Q. Huang, K. Sun, Y. Chi, J. Yan, Co-pyrolysis Characteristics and Kinetic Analysis of Organic Food Waste and Plastic, *Bioresource Technology*, Vol.249, 2018, pp. 16–23.

[29] Z. Xu, J.W. Albrecht, S.S. Kolapkar, S. Zinchik, E. Bar-Ziv, Chlorine Removal from U.S. Solid Waste Blends through Torrefaction. *Applied Sciences*, Vol.10, No.9, 2020, 3337, pp. 1-12.

[30] K. Sun, J. Qin, Z. Wang, Y. An, X. Li, B. Dong, X. Wu, Z. Guo, R. Fan, Polyvinyl alcohol/carbon Fibers Composites with Tunable Negative Permittivity Behavior, *Surfaces and Interfaces*, Vol.21, 2020, 100735.

[31] S. Karimi, R. Gholipur, Tunable Negative Permittivity Performance of Bamboo-derived carbon/NiS_2/$(CoFe_2O_4)x$/PVC Metacomposites in Light-Dependent Resistor and Low-Frequency Reflector, *Sensors and Actuators A: Physical*, Vol.380, 2024, 116051.

[32] U. S. Geological Survey, Mineral Commodity Summaries, 2019, doi: 10.3133/70202434.

[33] Y. Zhang, C. Hu, W.S. Luo, Effects of pH Manipulation, Biological Reduction, and Plant Growth on Cu^{2+} and Zn^{2+} Removal from Mine Drainage Using Iron-Oxide-Enriched Red Earth Soils, *Clean - Soil, Air, Water*, Vol.42, 2014, pp. 1272–1279.

[34] H.M. Anawar, Sustainable Rehabilitation of Mining Waste and Acid Mine Drainage Using Geochemistry, Mine Type, Mineralogy, Texture, Ore Extraction and Climate Knowledge, *Journal of Environmental Management*, Vol.158, 2015, pp. 111–121.

[35] V.A. Alekseenko, J. Bech, A.V. Alekseenko, N.V. Shvydkaya, N. Roca, Environmental Impact of Disposal of Coal Mining Wastes on Soils and Plants in Rostov Oblast, Russia, *Journal of Geochemical Exploration*, Vol.184, 2018, pp. 261–270.

[36] M.A. Khan, M.M. Alam, M. Naushad, Z.A. Alothman, M. Kumar, T. Ahamad, Sol-gel Assisted Synthesis of Porous Nano-Crystalline $CoFe_2O_4$ Composite and its Application in the Removal of Brilliant Blue-R from Aqueous Phase: An Ecofriendly and Economical Approach, *Chemical Engineering Journal*, Vol.279, 2015, pp. 416–424.

[37] S.B. Hearn, M.N. Dobbins, Slon Magnetic Separator: A New Approach for Recovering and Concentrating Iron Ore Fines, *Montreal Energy and Mines*, April 29- May 2, 2007.

[38] Y. Rajshekar, T.C. Alex, D.P. Sahoo, G.A. Babu, V. Balakrishnan, T. Venugopalan, S. Kumar, Iron Ore Slime as an Alternate Coolant in Steelmaking: Performance Evaluation at Commercial Scale, *Journal of Cleaner Production*, Vol.139, 2016, pp. 886–893.

[39] M. Jaishankar, T. Tseten, N. Anbalagan, B.B. Mathew, K.N. Beeregowda, Toxicity, Mechanism and Health Effects of Some Heavy Metals, *Interdisciplinary Toxicology,* Vol.7, 2014, pp. 60–72.

[40] F.J.D. Lopez, C. Montalvo, A Comprehensive Review of the Evolving and Cumulative Nature of Eco-Innovation in the Chemical Industry, *Journal of Cleaner Production*, Vol.102, 2015, pp. 30–43.

[41] L. Levidow, P. Lindgaard-Jørgensen, Å. Nilsson, S.A. Skenhall, D. Assimacopoulos, Process eco-Innovation: Assessing Meso-Level Eco-Efficiency in Industrial Water-Service Systems, *Journal of Cleaner Production*, Vol.110, 2016, pp. 54–65.

[42] G. Da Costa Cunha, J.A. Peixoto, D.R. De Souza, L.P.C. Rom˜ao, Z.S. Macedo, Recycling of Chromium Wastes from the Tanning Industry to Produce Ceramic Nanopigments, *Green Chemistry*, Vol.18, No.19, 2016, pp. 5342-5356.

[43] Y. Zhang, S. Duan, J. Li, S. Shao, W. Wang, S. Zhang, Life Cycle Assessment of Industrial Symbiosis in Songmudao Chemical Industrial Park, Dalian, China, *Journal of Cleaner Production,* Vol.158, 2017, pp. 192–199.

[44] T. Hu, L.M. Yang, Z.Y. Lu, X.G. Zheng, J.R. Zhou, X.P. Liu, C.L. Ni, Syntheses, Crystal Structures, And Magnetic Properties of Two New Organic-Inorganic Hybrid Materials Containing Metal-Bis(Dithiolene) Anion and Substituted Triphenylphosphinium, *Synthetic Metals*, Vol.227, 2017, pp. 131–138.

[45] M. Minella, D. Fabbri, P. Calza, C. Minero, Selected Hybrid Photocatalytic Materials for the Removal of Drugs from Water, *Current Opinion in Green and Sustainable Chemistry*, Vol.6, 2017, pp. 11–17.

[46] X. Zhang, J.Y. Dai, W. Lu, H.L.W. Chan, B. Wu, D.X. Li, A Novel Nanostructure and Multiferroic Properties in $Pb(Zr_{0.52}Ti_{0.48})O_3/CoFe_2O_4$ Nanocomposite Films Grown by Pulsed-Laser Deposition, *Journal of Physics D: Applied Physics,* Vol.41, No.23, 2008, 235405.

[47] A. Charris-Hernández, R. Melgarejo, D. Barrionuevo, A. Kumar, M.S. Tomar, Multiferroic Properties of $CoFe_2O_4/Bi_{3.4}La_{0.6}$ Ti_3O_{12} Bilayer Structure at Room Temperature, *Journal of Applied Physics*, Vol.114, No.3, 2013, 034108.

[48] D.M., Ghone, V.L. Mathe, K.K. Patankar, S.D. Kaushik, Microstructure, Lattice Strain, Magnetic and Magnetostriction Properties of Holmium Substituted Cobalt Ferrites Obtained by Co-Precipitation Method, *Journal of Alloys and Compounds*, Vol.739, 2018, pp. 52-61.

[49] R. Ahmad, I. Hussain Gul, M. Zarrar, H. Anwar, M.B. Khan Niazi, A. Khan, Improved Electrical Properties of Cadmium Substituted Cobalt Ferrites Nano-Particles for Microwave Application, *Journal of Magnetism and Magnetic Materials*, Vol.405, 2016, pp. 28-35.

[50] K. Maaz, S. Karim, A. Mashiatullah, J. Liu, M.D. Hou, Y.M. Sun, J.L. Duan, H.J. Yao, D. Mo, Y.F. Chen, Structural Analysis of Nickel Doped Cobalt Ferrite Nanoparticles Prepared by Coprecipitation Route, *Physica B: Condensed Matter*, Vol.404, No.21, 2009, pp. 3947-3951.

[51] S. Torkian, A. Ghasemi, R.S. Razavi, Cation Distribution and Magnetic Analysis of Wideband Microwave Absorptive CoxNi1−xFe_2O_4 Ferrites, *Ceramics International*, Vol.43, No.9, 2017, pp. 6987-6995.

[52] A.-H. El Foulani, A. Aamouche, F. Mohseni, J.S. Amaral, D.M. Tobaldi, R.C. Pullar, Effect of Surfactants on the Optical and Magnetic Properties of Cobalt-Zinc Ferrite

$Co_{0.5}Zn_{0.5}Fe_2O_4$, *Journal of Alloys and Compounds*, Vol.774, 2019, pp. 1250-1259.

[53] K.M. Srinivasamurthy, J.V. Angadi, S.P. Kubrin, S. Matteppanavar, D.A. Sarychev, P.M. Kumar, H.W. Azale, B. Rudraswamy, Tuning of Ferrimagnetic Nature and Hyperfine Interaction of Ni^{2+} Doped Cobalt Ferrite Nanoparticles for Power Transformer Applications, *Ceramics International*, Vol.44, No.8, 2018, pp. 9194-9203.

[54] A.B. Nawale, N.S. Kanhe, S.A. Raut, S.V. Bhoraskar, A.K. Das, V.L. Mathe, Investigation of Structural, Optical and Magnetic Properties of Thermal Plasma Synthesized Ni-Co Spinel Ferrite Nanoparticles. *Ceramics International*, Vol.43, No.9, 2017, pp. 6637-6647.

[55] S. Joshi, V.B. Kamble, M. Kumar, A.M. Umarji, G. Srivastava, Nickel Substitution Induced Effects on Gas Sensing Properties of Cobalt Ferrite Nanoparticles. *Journal of Alloys and Compounds*, Vol.654, 2016, pp. 460-466.

[56] A.-L. Gurgel, A.E. Martinelli, O.L. de Aquino Conceição, M.M. Xavier Jr., M.A.M. Torres, D.M. de Araújo Melo, Microwave-assisted Hydrothermal Synthesis and Magnetic Properties of Nanostructured Cobalt Ferrite. *Journal of Alloys and Compounds*, Vol.799, 2019, pp. 36-42.

[57] Y. Bi, Y. Ren, F. Bi, T. He, Water-assisted and Surfactant-Free Synthesis of Cobalt Ferrite Nanospheres via Solvothermal Method, *Journal of Alloys and Compounds*, Vol.646, 2015, pp. 827-832.

[58] M. Sajjia, M. Oubaha, T. Prescott, A.G. Olabi, Development of Cobalt Ferrite Powder Preparation Employing the Sol–Gel Technique and its Structural Characterization, *Journal of Alloys and Compounds*, Vol.506, No.1, 2010, pp. 400-406.

[59] Y.I. Kim, D. Kim, C.S. Lee, Synthesis and Characterization of $CoFe_2O_4$ Magnetic Nanoparticles Prepared by Temperature-controlled Coprecipitation Method, *Physica B*, Vol.337, 2003, pp. 42-51.

[60] M.S. Khandekar, R.C. Kambale, J.Y. Patil, Y.D. Kolekar, S.S. Suryavanshi, Effect of Calcination Temperature on the Structural and Electrical Properties of Cobalt Ferrite Synthesized by Combustion Method, *Journal of Alloys and Compounds*, Vol.509, No.5, 2011, pp. 1861-1865.

[61] P. Monisha, P. Priyadharshini, S.S. Gomathi, K. Pushpanathan, Influence of Mn Dopant on the Crystallite Size, Optical and Magnetic Behaviour of $CoFe_2O_4$ Magnetic Nanoparticles, *Journal of Physics and Chemistry of Solids*, Vol.148, 2021a, 109654.

[62] P. Monisha, P. Priyadharshini, S.S. Gomathi, K. Pushpanathan, Ferro to Superparamagnetic Transition: Outcome of Ni Doping in Polyethylene Glycol Capped $CoFe_2O_4$ Nanoparticles, *Journal of Alloys and Compounds*, Vol.856, 2021b, 157447.

[63] M. Hashim, Alimuddin, S. Kumar, S.E. Shirsath, R.K. Kotnala, J. Shah, R. Kumar, Synthesis and Characterizations of Ni^{2+} Substituted Cobalt Ferrite Nanoparticles, *Materials Chemistry and Physics*, Vol.139, No.2–3, 2013, pp. 364-374.

[64] R.S. Yadav, J. Havlica, J. Masilko, L. Kalina, J. Wasserbauer, M. Hajdúchová, V. Enev, I. Kuřitka, Z. Kožáková, Impact of Nd^{3+} in $CoFe_2O_4$ Spinel Ferrite Nanoparticles on Cation Distribution, Structural and Magnetic Properties, *Journal of Magnetism and Magnetic Materials*, Vol.399, 2016, pp. 109-117.

[65] R.S. Yadav, J. Havlica, M. Hnatko, P. Šajgalík, C. Alexander, M. Palou, E. Bartoníčková, M. Boháč, F. Frajkorová, J. Masilko, M. Zmrzlý, L. Kalina, M. Hajdúchová, V. Enev, Magnetic Properties of Co1-xZnxFe_2O_4 Spinel Ferrite Nanoparticles Synthesized by Starch-Assisted Sol-Gel Autocombustion Method and Its Ball Milling, *Journal of Magnetism and Magnetic Materials*, Vol.378, 2015, pp. 190-199.

[66] K. Kombaiah, J.J. Vijaya, L.J. Kennedy, M. Bououdina, R.J. Ramalingam, H.A. Al-Lohedan, Okra extract-assisted Green Synthesis of $CoFe_2O_4$ Nanoparticles and their Optical, Magnetic, and Antimicrobial Properties, *Ceramics International*, Vol.43, No.10, 2017, pp. 7682-7689.

[67] J. Chen, Y. Wang, Y. Deng, Highly Ordered $CoFe_2O_4$ Nanowires Array Prepared via a Modified Sol–Gel Templated Approach and Its Optical and Magnetic Properties, *Journal of Alloys and Compounds*, Vol.552, 2013, pp. 65-69.

[68] J. Revathi, M.J. Abel, V. Archana, T. Sumithra, R. Thiruneelakandan, J.J. Prince, Synthesis and Characterization of $CoFe_2O_4$ and Ni-doped $CoFe_2O_4$ Nanoparticles by Chemical Co-Precipitation Technique for Photo-Degradation of Organic Dyestuffs Under Direct Sunlight, *Physica B: Condensed Matter*, Vol.587, 2020, 412136.

[69] B.J. Rani, M. Ravina, B. Saravanakumar, G. Ravi, V. Ganesh, S. Ravichandran, R. Yuvakkumar, Ferrimagnetism in Cobalt Ferrite

($CoFe_2O_4$) Nanoparticles, *Nano-Structures & Nano-Objects*, Vol.14, 2018, pp. 84-91.

[70] B. Pourgolmohammad, S.M. Masoudpanah, M.R. Aboutalebi, Effects of the Fuel Type and Fuel Content on the Specific Surface Area and Magnetic Properties of Solution Combusted $CoFe_2O_4$ Nanoparticles, *Ceramics International*, Vol.43, No.11, 2017, pp. 8262-8268.

[71] M. Rani, U. Shanker Rachna, Efficient Photocatalytic Degradation of Bisphenol a by Metal Ferrites Nanoparticles under Sunlight, *Environmental Technology & Innovation*, Vol.19, 2020, 100792.

[72] R. Sharma, S. Singhal, Spinel Ferrite Mediated Photo-Fenton Degradation of Phenolic Analogues: A Detailed Study Employing Two Distinct Inorganic Oxidants, *Clean - Soil, Air Water*, Vol.46, No.1, 2018, 1700605.

[73] L. Li, Y. Xu, D. Zhong, N. Zhong, CTAB-surface-functionalized Magnetic MOF@ MOF Composite Adsorbent for Cr(VI) Efficient Removal from Aqueous Solution, *Colloids and Surfaces A: Physicochemical and Engineering Aspects*, Vol.586, 2020, 124255.

[74] K.K. Kefeni, B.B. Mamba, T.A.M. Msagati, Magnetite and Cobalt Ferrite Nanoparticles Used as Seeds for Acid Mine Drainage Treatment, *Journal of Hazardous Materials*, Vol.333, 2017, pp. 308–318.

[75] H. Panda, N. Tiadi, M. Mohanty, C.R. Mohanty, Studies on Adsorption Behavior of an Industrial Waste for Removal of Chromium from Aqueous Solution, *South African Journal of Chemical Engineering*, Vol.23, 2017, pp. 132-138.

[76] R. Thekkathu, D. Ashok, P.K. Ramkollath, S. Neelakandapillai, L.P. Kurishunkal, M.S.P. Yadav, N. Kalarikkal, Magnetically Recoverable $Ir/IrO_2@Fe_3O_4$ core/ SiO_2 Shell Catalyst for the Reduction of Organic Pollutants in Water, *Chemical Physics Letters*, Vol.742, 2020, 137147.

[77] J.A.S. Costa, R.A. de Jesus, C.M.P. da Silva, L.P.C. Romao, Efficient Adsorption of a Mixture of Polycyclic Aromatic Hydrocarbons (PAHs) by Si–MCM–41 Mesoporous Molecular Sieve, *Powder Technology*, Vol.308, 2017, pp. 434–441.

[78] J.H.F. de Jesus, G. da C. Cunha, E.M.C. Cardoso, A.S. Mangrich, L.P.C. Romão, Evaluation of Waste Biomasses and their Biochars for Removal of Polycyclic Aromatic Hydrocarbons, *Journal of Environmental Management*, Vol.200, 2017, pp. 186–195.

[79] V.C.L. de Barros Caetano, G. da Costa Cunha, R.V.M. Oliveira, M. da Rosa Alexandre, L.P.C. Romao, Magnetic Hybrid Support for Ultrasound-Assisted Magnetic Solid-Phase Extraction of Polycyclic Aromatic Hydrocarbons from Produced Water, *Microchemical Journal*, Vol.146, 2019, pp. 1195-1203.

[80] D.R.S. Cruz, B.T.J. Santos, G.C. Cunha, L.P.C. Romao, Green Synthesis of a Magnetic Hybrid Adsorbent ($CoFe_2O_4$/NOM): Removal of Chromium from Industrial Effluent and Evaluation of the Catalytic Potential of Recovered Chromium Ions, *Journal of Hazardous Materials*, Vol.334, 2017, pp. 76–85.

[81] P. Laokul, V. Amornkitbamrung, S. Seraphin, S. Maensir, Characterization and Magnetic Properties of Nanocrystalline $CuFe_2O_4$, Ni Fe_2O_4, Zn Fe_2O_4 Powders Prepared by the Aloe Vera Extract Solution, *Current Applied Physics*, Vol.11, 2011, pp. 101-108.

[82] R.V.M. Oliveira, A.F. Santos, M.D. Lima Santos, G. da Costa Cunha, L.P.C. Romão, Magnetic Solid-Phase Extraction of Bisphenol A from Water Samples Using Nanostructured Material Based on Graphene with Few Layers and Cobalt Ferrite, *Microchemical Journal*, Vol.181, 2022, 107741.

[83] K.H. Tan, *Humic Matter in Soil and the Environment: Principles and Controversies*, CRC Press, 2014.

[84] D.R.S. Cruz, B.T.J. Santos, G. da Costa Cunha, L.P.C. Romão, Green Synthesis of a Magnetic Hybrid Adsorbent ($CoFe_2O_4$/NOM): Removal of Chromium from Industrial Effluent and Evaluation of the Catalytic Potential of Recovered Chromium Ions, *Journal of Hazardous Materials*, Vol.334, 2017, pp. 76–85.

[85] L.P.C. Romão, J.R. Lead, J.C. Rocha, L.C. de Oliveira, A.H. Rosa, A.G.R. Mendonça, A. de S. Ribeiro, Structure and Properties of Brazilian Peat: Analysis by Spectroscopy and Microscopy, *Journal of the Brazilian Chemical Society*, Vol.18, 2007, pp. 714-720.

[86] G. da Costa Cunha, L.P.C. Romão, Z.S. Macedo. Production of Alpha-Alumina Nanoparticles Using Aquatic Humic Substances, *Powder Technology*, Vol.254, No.65, 2014, pp. 344-351.

[87] G. da Costa Cunha, D. Goveia, L.P.C. Romão, L.C. de Oliveira, Effect of the Competition of Cu(II) and Ni(II) on the Kinetic and Thermodynamic Stabilities of Cr(III)-Organic Ligand Complexes Using Competitive Ligand

Exchange (EDTA), *Journal of Environmental Management*, Vol.154, 2015, pp. 259-265.

[88] A. Goyal, S. Bansal, S. Singhal, Facile Reduction of Nitrophenols: Comparative Catalytic Efficiency of MFe_2O_4 (M = Ni, Cu, Zn) Nano Ferrites, *International Journal of Hydrogen Energy*, Vol.39, No.10, 2014, pp. 4895-4908.

[89] J.H. Zar, Biostatistical Analysis, Prentice-Hall, Englewood Cliffs, 1984.

[90] Statgraphics Centurion XV, sofware, StatPoint Inc, Statgraphics Centurion XV, Herndon, VA, USA, 2005.

[91] J.D. Hem; W.H. Cropper. *Chemistry of Iron in Natural Water*, Washington, U.S. Govt. Print. Off., Washington,1962.

[92] J. Pertusatti, A.G.S. Prado, Buffer Capacity of Humic Acid: Thermodynamic Approach, *Journal of Colloid and Interface Science*, 2007, Vol.314, No.2, 2007, pp. 484-489.

[93] U. Kurtan, Md. Amir, A. Yıldız, A. Baykal, Synthesis of Magnetically Recyclable $MnFe_2O_4$@SiO_2@Ag nanocatalyst: Its High Catalytic Performances for Azo Dyes and Nitro Compounds Reduction, *Applied Surface Science,* Vol.376, 2016, pp. 16-25.

[94] S. Amir, A. Jouraiphy, A. Meddich, M. El Gharous, P. Winterton, M. Hafidi, Structural Study of Humic Acids During Composting of Activated Sludge-Green Waste: Elemental analysis, FTIR and 13C NMR, *Journal of Hazardous Materials*, Vol.177, No.1–3, 2010, pp. 524-529.

[95] M.D. Landgraf, S.C. da Silva, M.O.O. Rezende, Mechanism of Metribuzin Herbicide Sorption by Humic Acid Samples from Peat and Vermicompost, *Analytica Chimica Acta*, Vol.368, No.1–2, 1998, pp. 155-164.

[96] X. Li, C. Wang, Y. Zeng, P. Li, T. Xie, Y. Zhang, Bacteria-assisted Preparation of Nano α-Fe_2O_3 Red Pigment Powders from Waste Ferrous Sulfate, *Journal of Hazardous Materials*, Vol.317, 2016, pp. 563-569.

[97] N. Papassiopi, K. Vaxevanidou, C. Christou, E. Karagianni, G.S.E. Antipas, Synthesis, Characterization and Stability of Cr(III) and Fe(III) Hydroxides, *Journal of Hazardous Materials*, Vol.264, 2014, pp. 490-497.

[98] F.J. Rodríguez, P. Schlenger, M. García-Valverde, Monitoring Changes in the Structure and Properties of Humic Substances Following Ozonation Using UV-Vis, FTIR and 1H NMR Techniques, *Science of The Total Environment*, Vol.541, 2016, pp. 623-637.

[99] D.C. Culita, C.M. Simonescu, M. Dragne, N. Stanica, C. Munteanu, S. Preda, O. Oprea, Effect of Surfactant Concentration on Textural, Morphological and Magnetic Properties of $CoFe_2O_4$ Nanoparticles and Evaluation of their Adsorptive Capacity for Pb(II) Ions, *Ceramics International,* Vol.41, No.10, Part A, 2015, pp. 13553-13560.

[100] S.H. Lee, Y.H. Jang, D.D. Nguyen, S.W. Chang, S.C. Kim, S.M. Lee, S.S. Kim, Adsorption Properties of Arsenic on Sulfated TiO_2 Adsorbents, *Journal of Industrial and Engineering Chemistry*, Vol.80, 2019, pp. 444–449.

[101] G.S. An, D.H. Chae, J.U. Hur, A.H. Oh, H.H. Choi, S.C. Choi, Y.S. Oh, Y.G. Jung, Hollow-structured Fe_3O_4@SiO_2 Nanoparticles: Novel Synthesis and Enhanced Adsorbents for Purification of Plasmid DNA, *Ceramics International*, Vol.44, 2018, pp. 18791–18795.

[102] R.G. Flores, S.L.F. Andersen, L.K.K. Maia, H.J. Jos´e, R. de F.P.M. Moreira, Recovery of Iron Oxides from Acid Mine Drainage and Their Application as Adsorbent or Catalyst, *Journal of Environmental Management*, Vol.111, 2012, pp. 53-60.

[103] V. Srivastava, T. Kohout, M. Sillanpa, Potential of Cobalt Ferrite Nanoparticles ($CoFe_2O_4$) for Remediation of Hexavalent Chromium from Synthetic and Printing Press Wastewater, *Journal of Environmental Chemical Engineering*, Vol.4, 2016, pp. 2922–2932. *Society*, Vol.7, 2010, pp. 1–37.

[104] M. Faraji, Y. Yamini, M. Rezaee, Magnetic Nanoparticles: Synthesis, Stabilization, Functionalization, Characterization, and Applications, *Journal of the Iranian Chemical Society,* Vol.7, 2010, pp. 1-37.

[105] S. Zhang, H. Niu, Y. Cai, X. Zhao, Y. Shi, Arsenite and Arsenate Adsorption on Coprecipitated Bimetal Oxide Magnetic Nanomaterials: $MnFe_2O_4$ and $CoFe_2O_4$. *Chemical Engineering Journal*., Vol.158, 2010, pp. 599-607.

[106] M.A. Khan, M.M. Alam, Mu. Naushad, Z.A. Alothman, M. Kumar, T. Ahamad, Sol–gel Assisted Synthesis of Porous Nano-Crystalline $CoFe_2O_4$ Composite and its Application in the Removal of Brilliant Blue-R from Aqueous Phase: An Ecofriendly and Economical Approach, *Chemical Engineering Journal*, Vol.279, 2015, pp. 416-424.

[107] P. Liu, H. Li, J. Wu, X. Wu, Y.i Shi, Z. Yang, K. Huang, X. Guo, S. Gao, Polystyrene Microplastics Accelerated Photodegradation of

Co-Existed Polypropylene via Photosensitization of Polymer Itself and Released Organic Compounds, *Water Research*, Vol.214, 2022, 118209.

[108] S. Klempová, M. Oravec, K. Vizárová, Analysis of Thermally and UV-Vis aged Plasticized PVC using UV-Vis, ATR-FTIR and Raman Spectroscopy, *Spectrochimica Acta, Part A: Molecular and Biomolecular Spectroscopy*. Vol.294, 2023, 122541.

[109] P. Paik, K.K. Kar, Thermal Degradation Kinetics and Estimation of Lifetime of Polyethylene Particles: 655 Effects of Particle Size, *Materials Chemistry and Physics*, Vol.113, 2009, pp. 953-961.

[110] M. Chen, J. Xu, R. Tang, S. Yuan, Y. Min, Q. Xu, P. Shi, Roles of Microplastic-Derived Dissolved 657 Organic Matter on the Photodegradation of Organic Micropollutants, *Journal of Hazardous Materials*, Vol.440, 2022, 129784.

[111] R.P. Pant, V. Kumar, S.K. Halder, S.K. Gupta, S. Singh, Investigations on Nanocrystalline Superparamagnetic Particles of $CoFe_2O_4$, *International Journal of Nanoscience*, Vol.6, No.6, 2007, pp. 515–519.

[112] D. Peddis, N. Yaacoub, M. Ferretti, A. Martinelli, G. Piccaluga, A. Musinu, C. Cannas, G. Navarra, J.M. Greneche, D. Fiorani, Cationic Distribution and Spin Canting in $CoFe_2O_4$ Nanoparticles, *Journal of Physics: Condensed Matter*, Vol.23, No.42, 2011, 426004.

[113] U. Shanker, V. Jassal, M. Rani, B.S. Kaith, Towards Green Synthesis of Nanoparticles: from Bio-Assisted Sources to Benign Solvents. A Review, *International Journal of Environmental Analytical Chemistry*, Vol.96, No.9, 2016, pp. 801–835.

[114] L. Gao, R. Li, X. Sui, R. Li, C. Chen, Q. Chen, Conversion of Chicken Feather Waste to N-Doped Carbon Nanotubes for the Catalytic Reduction of 4-Nitrophenol, *Environmental Science & Technology*, Vol.48, No.17, 2014, pp. 10191–10197.

[115] R. Huang, H. Zhu, R. Su, W. Qi, Z. He, Catalytic Membrane Reactor Immobilized with Alloy Nanoparticle-Loaded Protein Fibrils for Continuous Reduction of 4-Nitrophenol, *Environmental Science & Technology*, Vol.50, No.20, 2016, pp. 11263–11273.

[116] X.W. Han, S. Bi, W. Zhang, Z. Yang, One-Step Fabrication of Highly Dispersed Ag Nanoparticles Decorated N-Doped Reduced Graphene Oxide Heterogeneous Nanostructure for the Catalytic Reduction of 4-Nitrophenol, *Colloids and Surfaces A: Physicochemical and Engineering Aspects*, Vol.574, 2019, pp. 69–77.

[117] T. Kamal, S.B. Khan, A.M. Asiri, Nickel Nanoparticles-Chitosan Composite Coated Cellulose Paper: An Efficient and Easily Recoverable Dip-Catalyst for Pollutants Degradation, *Filter Environmental Pollution*, Vol.218, 2016, pp. 625–633.

[118] F. Sharifianjazi, M. Moradi, N. Parvin, A. Nemati, A. Jafari Rad, N. Sheysi, A. Abouchenari, A. Mohammadi, S. Karbasi, Z. Ahmadi, A. Esmaeilkhanian, M. Irani, A. Pakseresht, S. Sahmani, M. Shahedi Asl, Magnetic $CoFe_2O_4$ Nanoparticles Doped with Metal Ions: A Review, *Ceramics International Part B*, Vol.46, No.11, 2020, pp. 18391-18412.

[119] X. Guan, J. Chang, Z. Xu, Y. Chen, H. Fan, Remediation of Chromium(III)-contaminated Tannery Effluents by Using Gallic Acid-Conjugated Magnetite Nanoparticles, *RSC Advances*, Vol.6, No.35, 2016, pp. 29054–29063.

[120] Y. Guo, L. Zhang, X. Liu, B. Li, D. Tang, W. Liu, W. Qin, Synthesis of Magnetic Core- Shell Carbon dot@MFe_2O_4 (M = Mn, Zn and Cu) Hybrid Materials and Their Catalytic Properties, *Journal of Materials Chemistry A*, Vol.4, No.11, 2016, pp. 4044–4055.

[121] J. Feng, L. Su, Y. Ma, C. Ren, Q. Guo, X. Chen, $CuFe_2O_4$ Magnetic Nanoparticles: A Simple and Efficient Catalyst for the Reduction of Nitrophenol, *Chemical Engineering Journal*, Vol.221, 2013, pp. 16–24.

[122] Z. Hasan, D.W. Cho, C.M. Chon, K. Yoon, H. Song, Reduction of p-Nitrophenol by Magnetic Co-Carbon Composites Derived from Metal Organic Frameworks, *Chemical Engineering Journal*, Vol.298, 2016, pp. 183–190.

[123] Z.C. Zeledon-Toruno, C. Lao-Luque, F.X.C. de las Heras, M. Sole-Sardans, Removal of PAHs from water using an immature coal (leonardite), *Chemosphere*, Vol.67, 2007, pp. 505–512.

[124] L. Zan, S.L. Wang, W.J. Fa, Y.H. Hu, L.H. Tian, K.J. Deng, Solid-phase Photocatalytic Degradation of Polystyrene with Modified Nano-TiO_2 Catalyst, *Polymer*, Vol.47, 2006, pp. 8155-8162.

[125] P.J. Anderson, S. Warrack, V. Langen, J.K. Challis, M.L. Hanson, M.D. Rennie, Microplastic Contamination in Lake Winnipeg, Canada, *Environmental Pollution*, Vol.225, 2017, pp. 223-231.

[126] J. Sun, X.H. Dai, Q.L. Wang, M.C.M. van Loosdrecht, B.J. Ni, Microplastics in Wastewater Treatment Plants: Detection, Occurrence and Removal, *Water Research*, Vol.152, 2019, pp. 21-37.

[127] I. Nabi, A.U.R. Bacha, F. Ahmad, L.W. Zhang, Application of Titanium Dioxide for the Photocatalytic Degradation of Macro- and Micro-Plastics: A Review, *Journal of Environmental Chemical Engineering*, Vol.9, 2021, Article 105964.

[128] T. Thomas, N. Sandhyarani, Enhancement in the Photocatalytic Degradation of Low-Density Polyethylene-TiO_2 Nanocomposite Films Under Solar Irradiation, *RSC Advances*, Vol.3, 2013, pp. 14080-14087.

[129] K. Noro, Y. Kakimoto, Q. Wang, S. Akiyama, T. Takikawa, R. Omagari, Y. Yabuki, T. Amagai, Enhancement of Photodegradation of Polyethylene with Adsorbed Polycyclic Aromatic Hydrocarbons under Artificial Sunlight Irradiation, *Marine Pollution Bulletin*, Vol.194, 2023, 115331.

[130] S.W. Bigger, J. Scheirs, O. Delatycki, Effect of Light Intensity on the Photooxidation Kinetics of High-Density Polyethylene, *Journal of Polymer Science, Part A: Polymer Chemistry*, Vol.30, No.10, 1992, pp. 2277-2280.

[131] J.L. Philippart, C. Sinturel, R. Arnaud, J.L. Gardette, Influence of the Exposure Parameters on the Mechanism of Photooxidation of Polypropylene, *Polymer Degradation and Stability*, Vol.64, 1999, pp. 213-225.

[132] S. Therias, G. Rapp, C. Masson, J.-L. Gardette, Limits of UV-light Acceleration on the Photooxidation of Low-Density Polyethylene, *Polymer Degradation and Stability,* Vol.183, 2021, 109443.

[133] J.W. Martin, J.W. Chin, T. Nguyen, Reciprocity Law Experiments in Polymeric Photodegradation: A Critical Review, *Progress in Organic Coatings*, Vol.47, 2003, pp. 292-311.

[134] N. Khelidj, X. Colin, L. Audouin, J. Verdu, C. Monchy-Leroy, V. Prunier, Oxidation of Polyethylene Under Irradiation at Low Temperature and Low Dose Rate, Part II. Low Temperature Thermal Oxidation, *Polymer Degradation and Stability*, Vol.91, 2006, pp. 1598-1605.

[135] J. Pospısil, J. Pilar, N.C. Billingham, A. Marek, Z. Horak, S. Nespurek, Factors Affecting Accelerated Testing of Polymer Photostability, *Polymer Degradation and Stability*, Vol.91, 2006, pp. 417-422.

[136] A. Fairbrother, H.-C. Hsueh, J.H. Kim, D. Jacobs, L. Perry, D. Goodwin, C. White, S. Watson, L.-P. Sung, Temperature and Light Intensity Effects on Photodegradation of High-Density Polyethylene, *Polymer Degradation and Stability*, Vol.165, 2019, pp. 153-160.

[137] M.A.G. Bardi, M.M.L. Munhoz, R.A. Auras, L.D.B. Machado, Assessment of UV Exposure and Aerobic Biodegradation of Poly(Butylene Adipate-Co-Terephthalate)/Starch Blend Films Coated with Radiation-Curable Print Inks Containing Degradation-Promoting Additives, *Industrial Crops and Products*, Vol.60, 2014, pp. 326-334.

[138] Y. Zhu, Y. Zhai, S. Li, X. Liu, B. Wang, X. Liu, Y. Fan, H. Shi, C. Li, Y. Zhu, Thermal Treatment of Sewage Sludge: A Comparative Review of the Conversion Principle, Recovery Methods and Bioavailability-Predicting of Phosphorus, *Chemosphere*, Vol.291, Part 3, 2022, 133053.

[139] G. Rapp, J. Tireau, P.O. Bussiere, J.M. Chenal, F. Rousset, L. Chazeau, J.L. Gardette, S. Therias, Influence of the Physical State of a Polymer Blend on Thermal Ageing, *Polymer Degradation and Stability*, Vol.163, 2019, pp. 161-173.

[140] L. Ding, R. Mao, S. Ma, X. Guo, L. Zhu, High Temperature Depended on the Ageing Mechanism of Microplastics under Different Environmental Conditions and its Effect on the Distribution of Organic Pollutants, *Water Research*, Vol.174, 2020, Article 115634.

[141] C. Wang, Z. Xian, X. Jin, S. Liang, Z. Chen, B. Pan, B. Wu, Y.S. Ok, C. Gu, Photo-aging of Polyvinyl Chloride Microplastic in the Presence of Natural Organic Acids, *Water Research*, Vol.183, 2020, Article 116082.

[142] H. Wang, P. Liu, M. Wang, X. Wu, Y. Shi, H. Huang, S. Gao, Enhanced Phototransformation of Atorvastatin by Polystyrene Microplastics: Critical Role of Aging, *Journal of Hazardous Materials*, Vol.408, 2021, Article 124756.

[143] H. Wang, J. Zhu, Y. He, J. Wang, N. Zeng, X. Zhan, Photoaging Process and Mechanism of Four Commonly Commercial Microplastics, *Journal of Hazardous Materials*, Vol.451, 2023, 131151.

[144] X. Wu, P. Liu, H. Shi, H. Wang, H. Huang, Y. Shi, S. Gao, Photo Aging and Fragmentation of Polypropylene Food Packaging Materials in Artificial Seawater, *Water Research*, Vol.188, 2021, 116456.

[145] L. Zhou, T. Wang, G. Qu, H. Jia, L. Zhu, Probing the Aging Processes and Mechanisms of Microplastic under Simulated Multiple Actions Generated by Discharge Plasma, *Journal of Hazardous Materials*, Vol.398, 2020, 122956.

[146] S. Dong, X. Yan, Y. Yue, W. Li, W. Luo, Y. Wang, J. Sun, Y. Li, M. Liu, M. Fan, H_2O_2 Concentration Influenced the Photoaging Mechanism and Kinetics of Polystyrene Microplastic under UV Irradiation: Direct and Indirect Photolysis, *Journal of Cleaner Production*, Vol.380, Part 2, 2022, 135046.

Contribution of Individual Authors to the Creation of a Scientific Article (Ghostwriting Policy)

Prof. Dr. Delia Teresa Sponza and Post-Dr. Rukiye Öztekin took an active role in every stage of the preparation of this article.

The authors equally contributed in the present research, at all stages from the formulation of the problem to the final findings and solution.

Sources of Funding for Research Presented in a Scientific Article or Scientific Article Itself

The experimental phases of this research study were conducted at the National Research Council (NRC) of Canada, Research Centres, Ontario, Canada. The authors would like to thank this body for providing financial support.

Conflict of Interest

The authors have no conflicts of interest to declare that are relevant to the content of this article.

APPENDIX

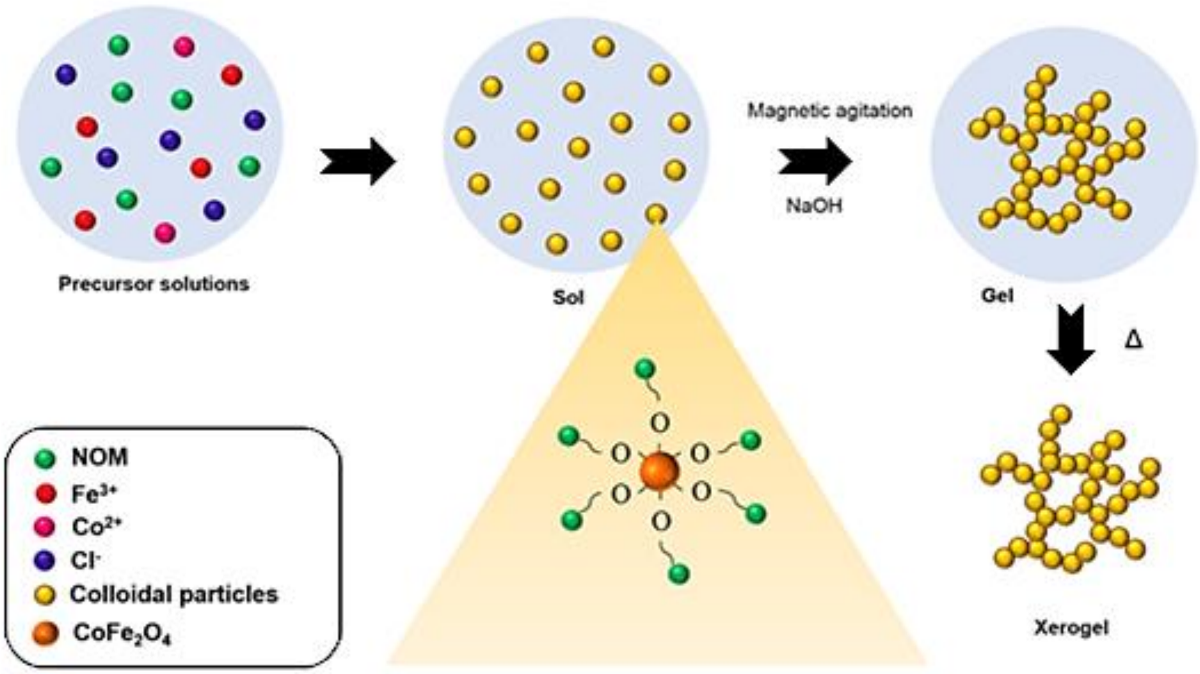

Fig. 1. The schematic illustration of the possible formation mechanism for the $CoFe_2O_4$/NOM nanocomposites (NOM: green sphere; Fe^{3+} ions: red sphere; Co^{2+} ions: pink sphere; Cl^- ions: blue sphere; Colloidal particles: yellow sphere; $CoFe_2O_4$: orange sphere, respectively), (adapted from Ref., [82]).

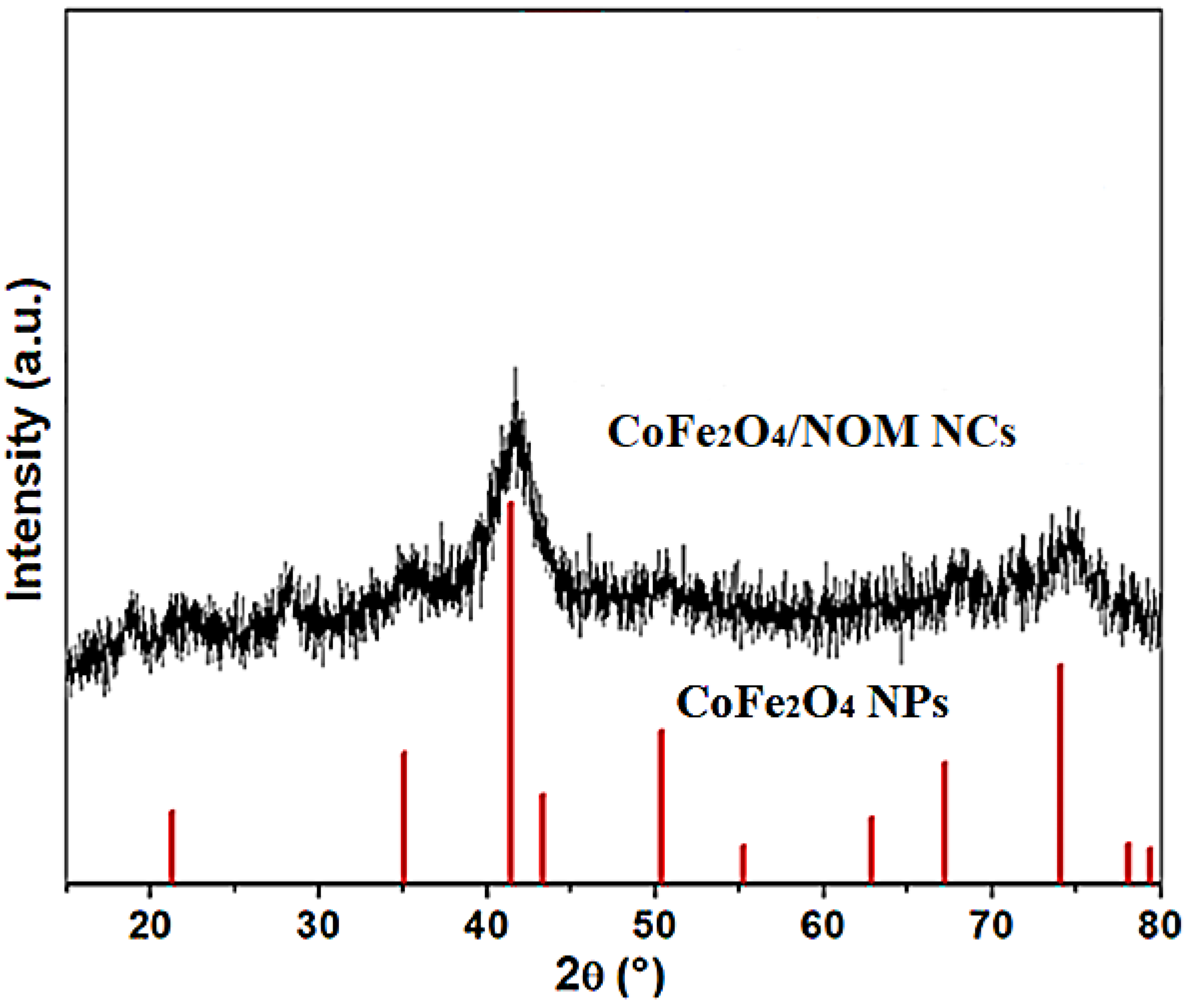

Fig. 2. XRD spectrum of the $CoFe_2O_4$/NOM NCs (black pattern), and comparison with the ICSD (no:192031) $CoFe_2O_4$ NPs standard (red pattern).

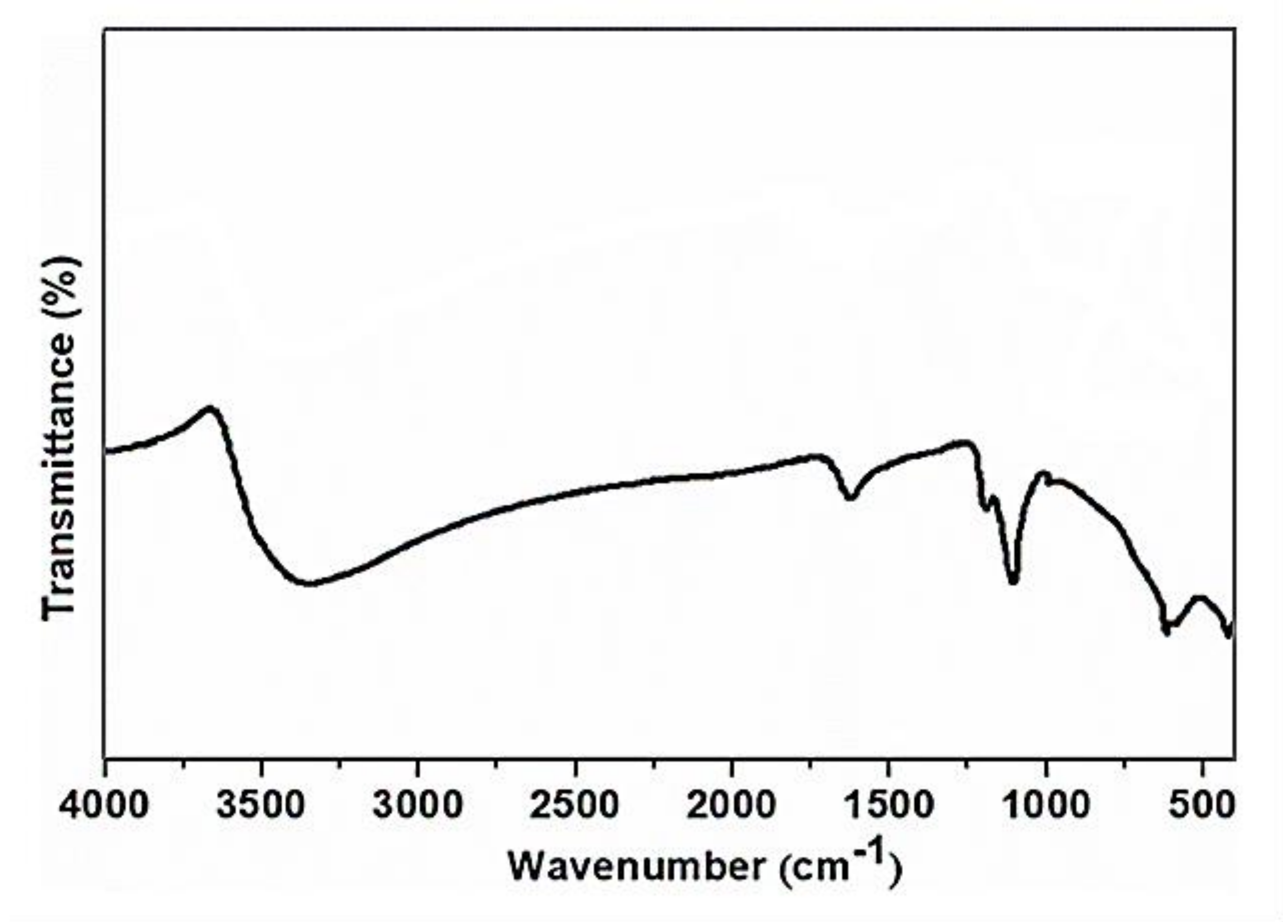

Fig. 3. FTIR spectrum of $CoFe_2O_4$/NOM NCs hybrid materials.

Table 1. Comparison of the results of the present study and those found in the literature for PE, PP, PS and PVC polymers using different catalysts.

Catalyst	Mass (mg/l)	PE yield (%)	PP yield (%)	PS yield (%)	PVC yield (%)	Time (min)	References
$Ag@TiO_2$	10	78	67	69	70	540	[118]
$Ni_{0.8}Cu_{0.2}Fe_2O_4$	15	87	80	76	72	120	[119]
Pt/CeO_2Co_{10}	0.15	70	69	66	69	240	[99]
C–dots@ $CuFe_2O_4$	0.05	65	70	60	74	60	[120]
$Pd/RGO/Fe_3O_4$	5	79	70	66	69	60	[121]
$CoFe_2O_4$/NOM NCs	10	99.90	99.90	98.20	98.20	30	In this work

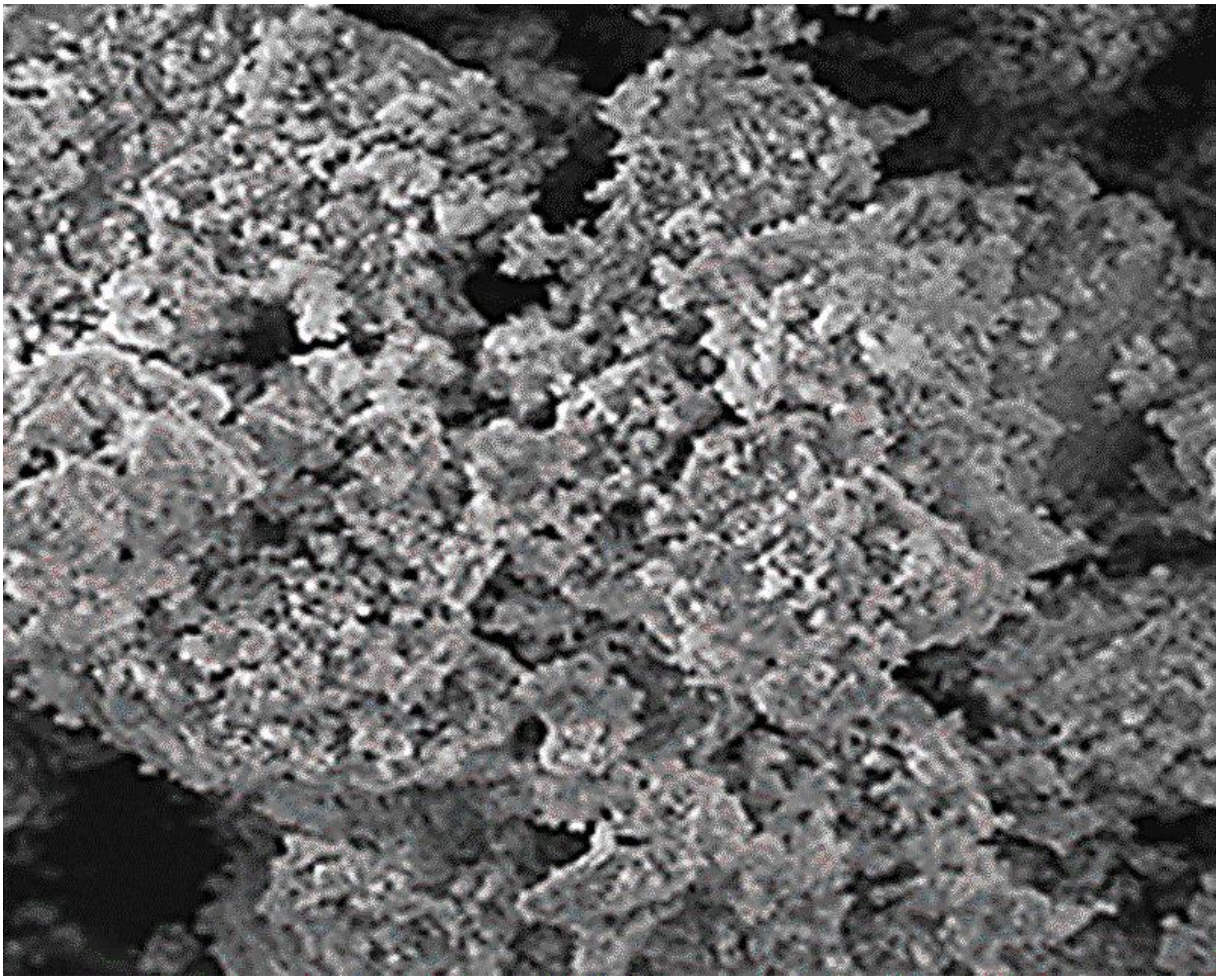

Fig. 4. FESEM image of $CoFe_2O_4$/NOM NCs hybrid materials (FESEM image size: 5 μm).

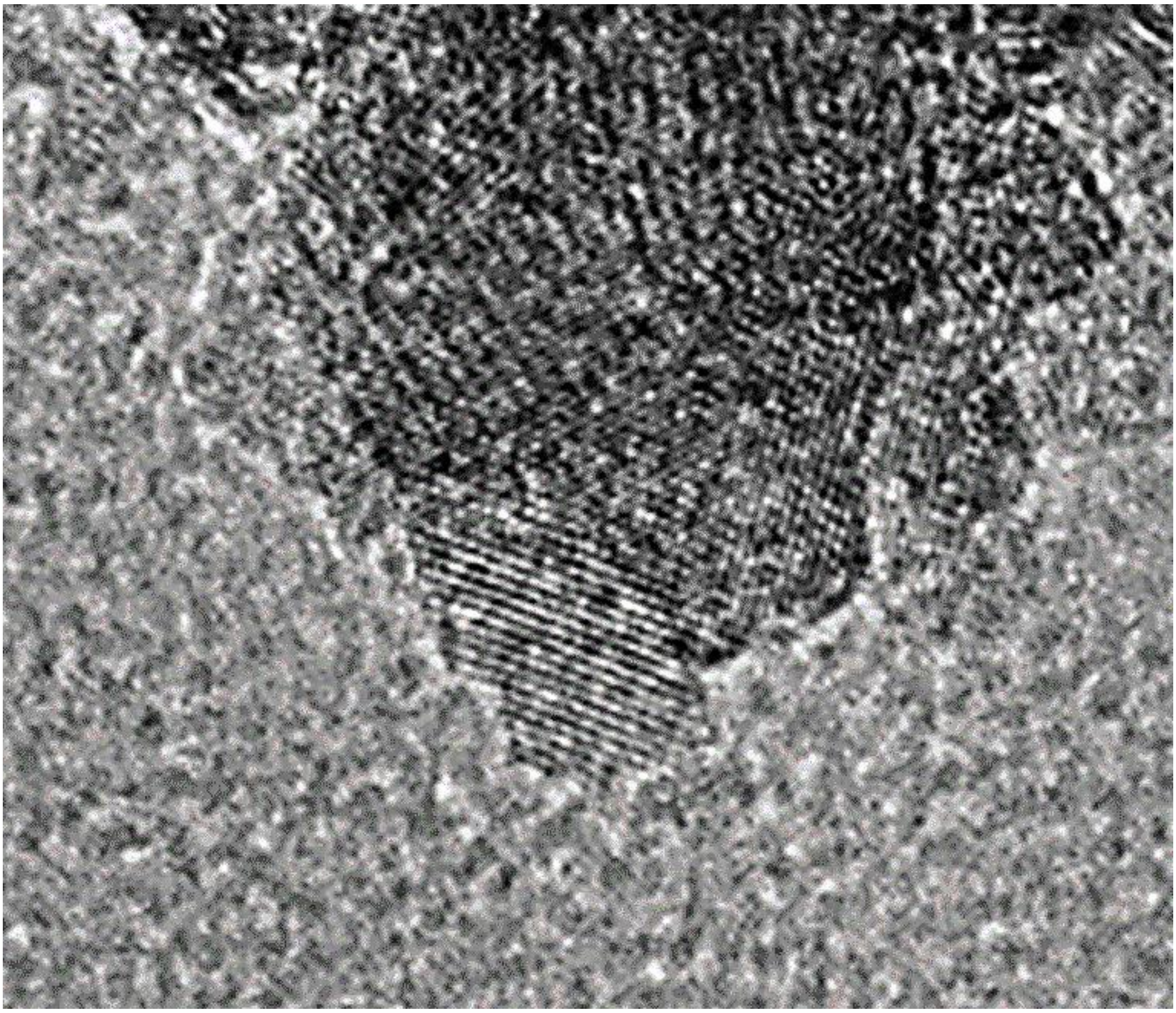

Fig. 5. HRTEM image of $CoFe_2O_4$/NOM NCs hybrid materials (HRTEM image size: 5 nm).

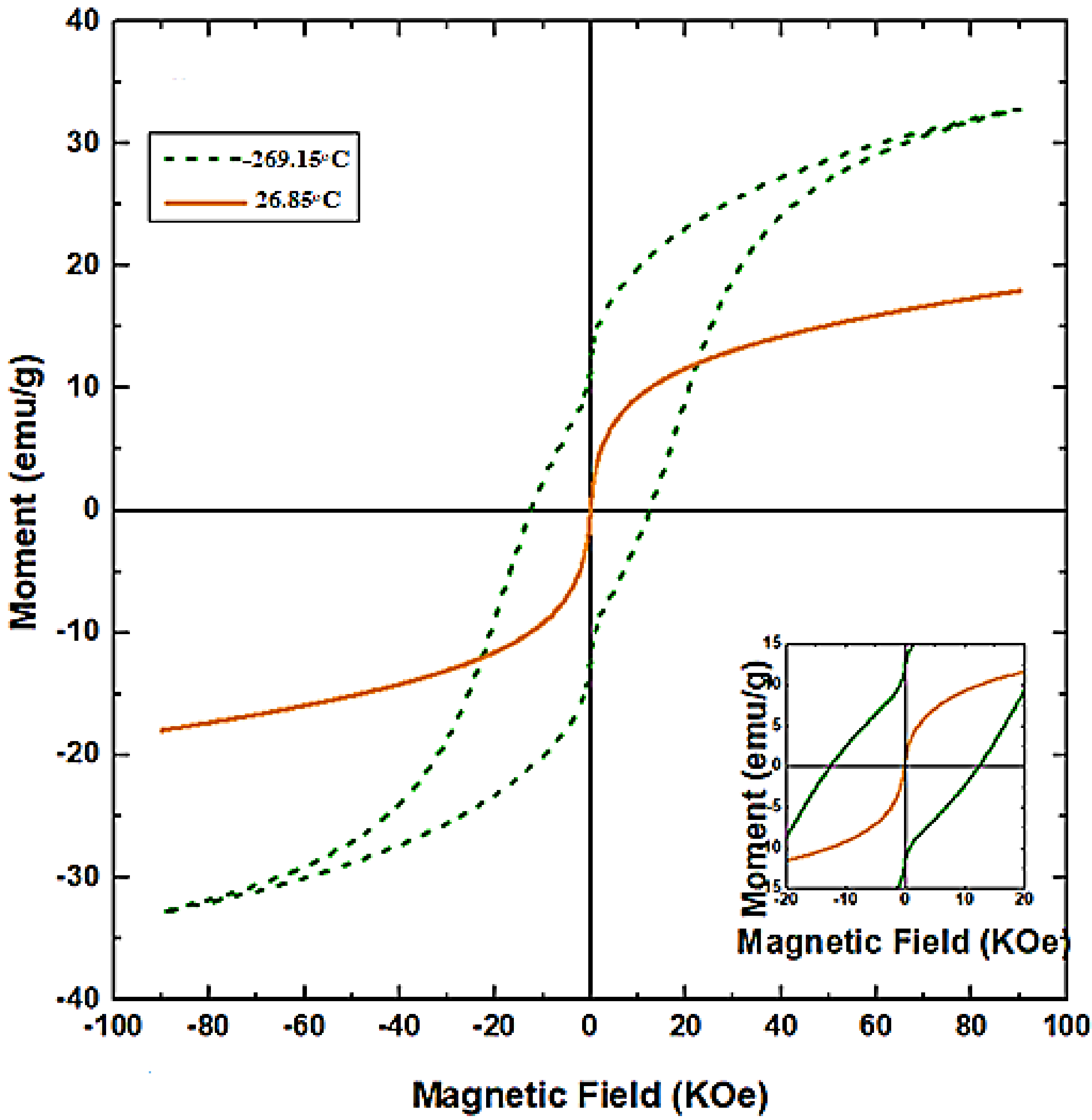

Fig. 6. Magnetization curves, as a function of the applied magnetic field, with a maximum field of ± 90 kOe at –269.15°C (dashed line) and at 26.85°C room temperature (solid line), for the sample of $CoFe_2O_4$/NOM NCs hybrid materials. The insert shows magnifications for Hc up to ± 5 kOe and ± 20 kOe, respectively.

Table 2. 1000 mg/l individual PE, PP, PS and PVC polymers removal percentages using the 10 mg/l $CoFe_2O_4$/NOM at an agitation speed of 150 rpm, at T = 25°C.

Time (min)	**Nanoplastics Removal Efficiencies (%)**			
	PE (%)	**PP (%)**	**PS (%)**	**PVC (%)**
30	99.90	99.90	99.90	99.20
30	99.90	99.90	99.90	99.20
30	99.90	99.90	99.90	99.20
30	99.90	99.90	99.90	99.20
30	99.90	99.90	99.90	99.20
30	99.90	99.90	99.90	99.20
30	99.90	99.90	99.90	99.90
30	99.90	99.90	99.90	99.90
30	99.90	99.90	99.90	99.90
30	99.90	99.90	99.90	99.90

Table 3. Variations of polymer yields versus pH.

pH	PE Yields (%)	PP Yields (%)	PS Yields (%)	PVC Yields (%)
2.0	53	45	43	50
3.0	56	43	46	49
4.0	78	80	82	79
7.0	99.90	99.90	99.90	99.20
9.0	43	40	39	40
11.0	32	28	22	30

Table 4. Variations of individual 1000 mg/l polymer yields versus $CoFe_2O_4$/NOM NCs concentrations after 30 min.

$CoFe_2O_4$/NOM NCs (mg/l)	PE Yields (%)	PP Yields (%)	PS Yields (%)	PVC Yields (%)
0.2	34	43	40	38
2	56	43	46	49
3	78	80	82	79
4	87	99	99	98
8	90	90	89	87
10	99.90	99.90	99.90	99.20
20	83	84	83	81
30	80	80	80	79

Table 5. Variations of polymer yields versus $CoFe_2O_4$ to NOM ratios in whole nanocomposite concentrations.

$CoFe_2O_4$ to NOM ratio (%)	PE Yields (%)	PP Yields (%)	PS Yields (%)	PVC Yields (%)
2	80	83	86	85
4.2	99.90	99.90	99.90	99.20
5	78	80	82	79
6	70	69	74	71

Table 6. Variations of polymer yields versus sun light powers

Sun light power (W/m^2)	PE Yields (%)	PP Yields (%)	PS Yields (%)	PVC Yields (%)
20	56	60	62	60
30	99.90	99.90	99.90	99.20
40	78	80	82	79
60	70	69	74	71

Table 7. Variations of polymer yields versus increasing temperature

Temperature (°C)	PE Yields (%)	PP Yields (%)	PS Yields (%)	PVC Yields (%)
20	59	69	68	66
30	99.90	99.90	99.90	99.20
40	90	90	90	88
60	80	79	80	81

Table 8. Variations of polymer yields versus aging procedure.

Surface Area of Nanocomposite (cm^2/g)	**PE Yields (%)**	**PP Yields (%)**	**PS Yields (%)**	**PVC Yields (%)**
165 (not aged)	80	79	76	75
420 (aged)	92	90	90	88
520 (aged)	99.90	99.90	99.00	99.90
188 (not aged)	86	80	80	79

Table 9. Reusability studies of $CoFe_2O_4$/NOM NC during 10 cycles for PE, PP, PS and PVC photodegradation yields with 10 mg/l $CoFe_2O_4$/NOM NC.

Cycles	10 mg/l $CoFe_2O_4$/NOM NC				
	Time (min)	Conversion (%) for PE	Conversion (%) for PP	Conversion (%) for PS	Conversion (%) for PVC
1	30	99.90	99.90	99.90	99.20
2	30	99.90	99.90	99.90	99.20
3	30	99.90	99.90	99.90	99.20
4	30	99.90	99.90	99.90	99.20
5	30	99.90	99.90	99.90	99.20
6	30	99.90	99.90	99.90	99.20
7	30	99.90	99.90	99.90	99.20
8	30	99.90	99.90	99.90	99.20
9	30	99.90	99.90	99.90	99.20
10	30	99.90	99.90	99.90	99.20

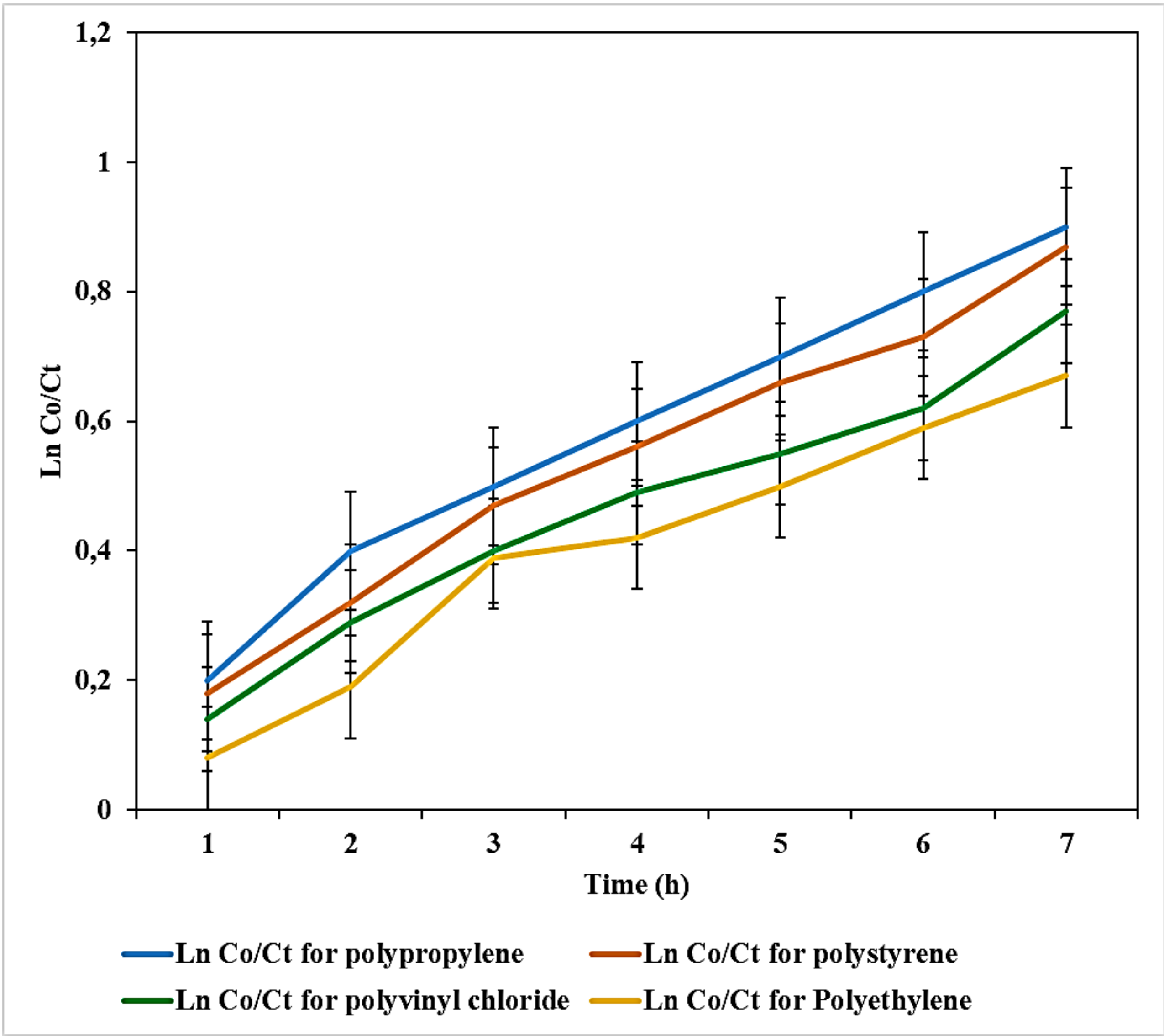

Fig. 7. Pseudo–first–order reaction kinetic of four polymers (PE, PP, PS and PVC).